ACS OMEGA

Article

http://pubs.acs.org/journal/acsodf

Remarkable Facet Selective Reduction of 4-Nitrophenol by Morphologically Tailored (111) Faceted Cu_2O Nanocatalyst

Teresa Aditya,[†] Jayasmita Jana,[†] Navin Kumar Singh,[†] Anjali Pal,[‡] and Tarasankar Pal*[,†]

[†]Department of Chemistry and [‡]Department of Civil Engineering, Indian Institute of Technology, Kharagpur 721302, India

Supporting Information

ABSTRACT: In this work, we have disclosed the facile syntheses of morphologically diverse Cu_2O nanoparticles using our laboratory designed modified hydrothermal reactor employing low-cost copper (II) acetate precursor compounds. The reaction conditions dovetail the effect of ethylene glycol (EG) and glucose to exclusively evolve the morphology tuned Cu_2O nanomaterial at different pHs. The morphology tuning produces octahedron (Oh), dwarf hexapod (DHP), and elongated hexapod (EHP) Cu_2O structures only with the optimized reagent concentrations. Interestingly, all of them were bestowed with a (111) facet, a superlative facet for facile nitroarene reduction. Thus, the morphology reliant catalytic reaction becomes evident. However, when used individually, EG and glucose evolve ill-defined CuO/Cu_2O and Cu_2O structures, respectively. We have observed that a change in pH of the medium at the onset of the reaction is obligatory for the evolution of tailor-made morphologically diverse Cu_2O nanoparticles. However, preformed Cu_2O particles do not suffer further structure/morphology changes under deliberate pH (6.0−9.0) change. With the as-obtained Oh, DHP, and EHP Cu_2O structures, we further delve into the realm of catalysis to understand the splendor of the nanocatalyst, morphology and surface area dependence, facet selective reactivity, and other factors affecting the catalytic efficiency. The remarkable rate of catalysis of 4-nitrophenol (4-NP), evident from the catalyst activity parameter (k_a = 123.6 g^{-1} s^{-1}), to produce 4-aminophenol in the presence of a reducing agent like sodium borohydride ($NaBH_4$) of the as-prepared catalysts is evidence of the collaborative effects of the effective surface area, surface positive charge, and active (111) facet of the Cu_2O nanocatalyst. We have also studied the effect of other common anions, namely, Cl^-, NO_2^-, NO_3^-, CO_3^{2-}, and SO_4^{2-} on the reduction process. To obtain a general consensus about facets, we compared (100) and (111) faceted Cu_2O nanocatalysts not only for 4-NP reduction but also for the reduction of toxic chromium Cr(VI) in the presence of formic acid to further emphasize the importance of facet selectivity in catalysis and the versatility of the morphology tuned as-prepared Cu_2O.

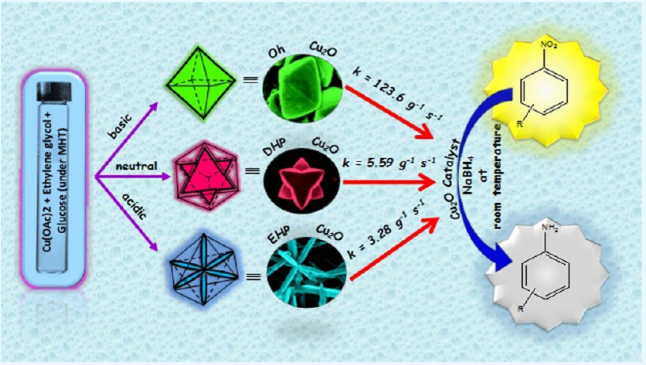

INTRODUCTION

In contemporary science, the morphology of nanomaterials has been instrumental in improving properties and catalytic efficiency.[1] Nanomaterials not only have novel electronic, optical, magnetic, chemical, and mechanical properties[2−4] in comparison with their bulk counterparts but these properties are also intimately related to their obtained morphology. This has attracted much attention focussing on new synthetic strategies, especially those for metal oxides. Cuprous oxide, a p-type semiconductor with a band gap of 2.2 eV, is available as the robust but only naturally occurring monovalent copper compound on earth.[5] A large amount of water insoluble Cu_2O is discarded after Fehling's test in academic and pathological laboratories. It has been widely exploited for catalysis, magnetic storage media, solar energy conversion, electrodes for lithium ion batteries, and gas sensors. To date, various structures of crystalline Cu_2O have been reported exploiting various reducing and capping agents resulting in fascinating octahedral, flowerlike, rod, cubic, and multipod structures.[6−14] In this work, we have judiciously employed glucose as a growth directing agent, ethylene glycol (EG) as the stabilizing agent, and both act collaboratively to reduce Cu(II) in a solution of copper acetate, in various proportions, to yield octahedral (Oh), dwarf hexapod (DHP) and elongated hexapod (EHP) structures under different pHs. This synergistic effect of EG and glucose was studied systematically. Thereby, the adept catalyst was then exploited in catalyzing various reactions, namely, nitroarene reduction and the reduction of Cr(VI) to Cr(III), to show its versatility. An insignificant amount of the as-synthesized Cu_2O catalyst was responsible for carrying out effective progress and completion of the reactions. Of the three morphologies, the Oh structure delivered the best catalysis owing to its greater surface area and surface charge. Facet selective theories were established with a comparative study of the two different

Received: November 30, 2016
Accepted: April 28, 2017
Published: May 10, 2017

DOI: 10.1021/acsomega.6b00447
ACS Omega 2017, 2, 1968−1984

reduction reactions by evaluation of the efficiency of the (111) facet in comparison to a (100)[15] facet.

Nitroaromatic compounds are an environmentally redundant material that are hazardous to living organisms. Pesticides containing nitroaromatic compounds show a hydrophobic nature and are not miscible in water, accumulating in sediments resulting in potential contamination. In environmental legislation, 4-nitrophenol (4-NP) has been recorded as a carcinogenic, teratogenic, and mutagenic element and hence is perilous to human life. The catalytic hydrogenation of nitroaromatic compounds has considerable significance as the aromatic amines produced are important intermediates and precursors required for production of different pharmaceuticals, polymers, herbicides, agrochemicals, pigments, and dyes.[16,17] The benchmark reaction of 4-NP reduction to test the catalytic efficiency of metal nanoparticles is widely used and was proposed by our group.[18−22] The convenience of the model reaction lies in the fact that the reaction proceeds at an infinitesimally slow rate without suitable catalyst and the progress of the reaction can be monitored with a UV−vis spectrophotometer when a suitable catalyst is introduced into the reaction mixture. It remains a challenging task to reduce nitro compounds in the presence of other reducible groups in the moiety. The reduction is initiated by $NaBH_4$ in the presence of noble metal catalysts.[23−26] The expense and low availability of such metals convinced us to meticulously design a suitable catalyst which is cost effective, earth-abundant, and nontoxic. However, to the best of our knowledge, this is the first report of a tailor-made synthesis of octahedral and hexapod nanostructures of Cu_2O from the combined effect of EG and glucose under a modified hydrothermal treatment (MHT)[27,28] but from variable pH. Herein, we reveal a high yielding green synthesis of Cu_2O nanostructures utilizing EG as the stabilizer and glucose as the growth directing agent individually, however both also work cooperatively as the reducing agent in the system at variable pH conditions. Thereafter, the remarkable efficiency of the as-synthesized proficient catalyst was attested from nitroarene reduction. We also found a linear relation between surface area and the rate constants for the three morphologies. Various anions (Cl^-, NO_2^-, NO_3^-, CO_3^{2-}, and SO_4^{2-}), five times diluted with respect to 4-NP, were introduced into the reaction mixture to observe the adeptness of the as-prepared catalyst to reduce 4-NP and to study the anion effect on the reaction rate. Our as-synthesized (111) faceted Oh Cu_2O nanocatalyst showed nitroarene reduction in a very short time span of 4−15 min, an unprecedented observation for a $\sim 10^{-4}$ M concentration of nitroarenes, leaving aside the morphologically different (111) or (100) faceted Cu_2O. The plausible mechanism instrumental in bringing about 4-NP reduction (k_a = 123.6 g^{-1} s^{-1}) was the collaborative effort of particle size, active surface area, facet, and surface potential. Catalysis for Cr(m, mVI) reduction (k_a = 2.0 g^{-1} s^{-1}) was also viable due to the efficiency and versatility of this unique inexpensive catalyst and the preferential activity of the (111) facet toward specific reactions.

RESULTS AND DISCUSSION

Analytical Instruments. Details are provided in the Supporting Information.

X-ray Diffraction (XRD) Analysis. The phase structure and purity of the as-prepared Cu_2O nanoparticles of the three different morphologies, namely, Oh, DHP, and EHP, obtained from the combined effect of glucose and EG were analyzed by X-ray diffraction study (Figure 1). The peaks at 2θ = 29.9, 36.5, 42.2, 52.6, 61.4, 73.8, and 77.4° can be indexed to the (110),

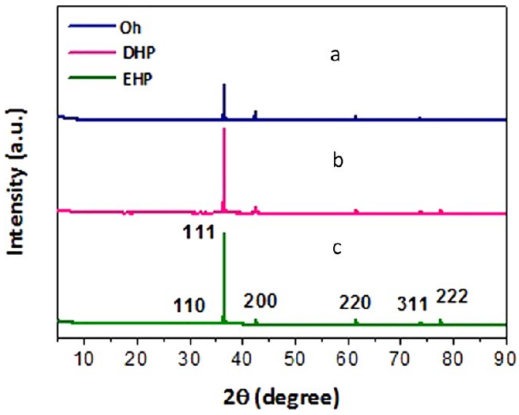

Figure 1. XRD patterns of Cu_2O: (a) Oh, (b) DHP, (c) EHP morphologies of Cu_2O.

(111), (200), (211), (220), (311), and (222) reflection peaks (JCPDS file 77-0199) attesting that the cubic Cu_2O crystal structure formed is phase pure. In all three cases, the (111) plane shows the most intense diffraction peak revealing the exposure of the (111) plane. From the 3D model, it was noted that the EG stabilizer exclusively stabilizes the (111) plane and hence a slow growth rate is the consequence. On the basis of the Gibbs−Wulff's theorem, the facets bestowed with higher surface energies always grow promptly and finally decrease or disappear from the eventual morphologies, whereas the crystal facets with lower surface energies grow in a sluggish pathway and are conserved in the ultimate structure.[29] Only the facet with a slower growth rate gets exposed to a large extent and shows an intense diffraction peak in the XRD pattern.[30] The predominant facet exposed in Oh is (111) due to the diminished growth on this plane and thus it shows a much higher diffraction intensity than that of the (200) planes in all three cases. In the spectra, the diffraction intensity ratios of (111)/(200) progressively increased in the following order Oh < DHP < EHP as a result of increasing (111) facets. In comparison, in the Cu_2O cube, the (100) plane is more exposed and hence the ratio is less, as is evident from Figure S1a in the Supporting Information. Cu_2O consists of a cuprite crystal structure with a body-centered cubic packing of oxygen atoms with a copper atom occupying half of the tetrahedral site. From the crystal model, it has been reported that (100) planes have oxygen atoms present in the unit cell, whereas slicing along the (111) plane exposes the Cu atoms with dangling bonds.[31] Hence, the (111) plane with Cu atoms exposed has a greater positive surface in comparison with that of the neutral (100) faces of the cube.[32] The growth mechanism was also studied with the help of time-dependent XRD (Figure S2) and it was confirmed that Cu_2O nuclei are formed that gradually evolve into various morphologies.

X-Ray Photoelectron Spectroscopy (XPS) Analysis. The oxidation state and surface atomic composition of the Oh, DHP, and EHP Cu_2O nanomaterials were investigated by wide range and high-resolution X-ray photoelectron spectroscopy, as shown in Figure 2. The observed symmetrical peaks are indicative of more than one chemical state of copper. Peaks of Cu $2p_{3/2}$ and Cu $2p_{1/2}$ at 932.6 and 952.7 eV, respectively, have been reported for Oh Cu_2O.[33] Apart from the main peak of

DOI: 10.1021/acsomega.6b00447
ACS Omega 2017, 2, 1968−1984

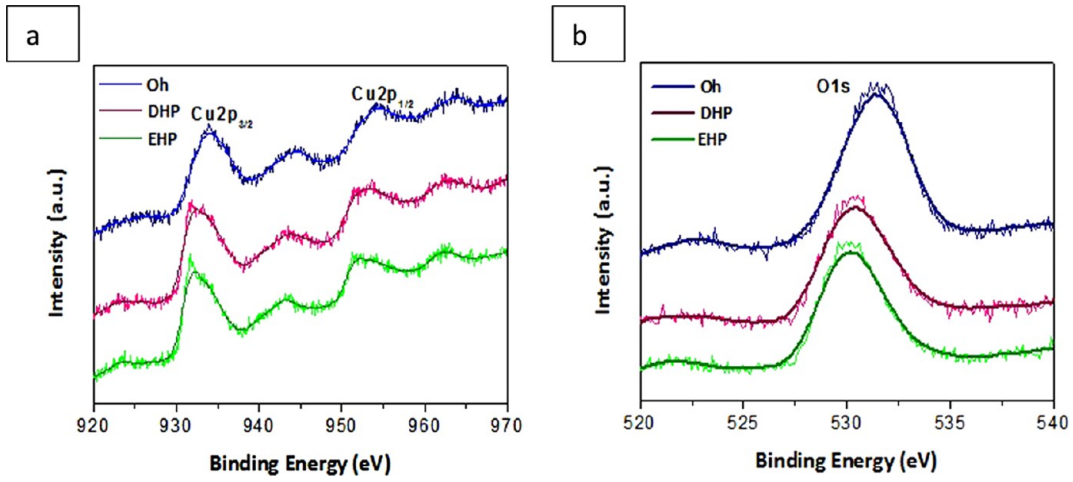

Figure 2. XPS spectra of the prepared Oh, DHP, and EHP (a) for Cu 2p and (b) for O 1s.

Cu(I), a few shakeup satellite peaks are observed in the spectra in a higher binding energy range at around 940.6 and 943.3 eV, which can be attributed to Cu(II)[34,35] states in CuO incorporated due to surface oxidation. Hence, this shows the presence of CuO on the surface of Cu_2O, although the XRD analysis proved only the presence of Cu_2O. In the case of DHP, the main peaks are at 931.2 and 951.8 eV; whereas, in the case of EHP they are at 930.7 and 951.2 eV. Hence, this change and decrease in binding energy suggests that with a decrease in alkalinity and increase in acidity, there is less CuO on the surface of the nanoparticle. Hence, in a more alkaline medium there is the possibility of more CuO by surface oxidation than that in acidic media. The corresponding O 1s peak for DHP and EHP at ~530.3 eV matched well with the literature value.[38] For the Oh sample, the main O 1s peak is centered at a higher binding energy value of 531.5 eV. This was assigned to the adsorbed O on the surface on Cu_2O due to the presence of hydroxyl groups, which may be due to the precursor NaOH added during the synthesis. The Auger spectral analysis [Figure S3a] after surface cleaning shows a peak at 916.9 eV which is a clear indication of the Cu(I) present in the as-synthesized samples.[36,37] Also, to confirm this, we further applied XPS to our Oh catalyst after sputtering and observed that the peak of the CuO satellites vanished with intense Cu_2O peaks confirming the presence of CuO is on the surface only [Figure S3b].

Fourier Transform Infrared (FTIR) Analysis. The FTIR spectra of the as-prepared Cu_2O synthesized from its precursor glucose and copper acetate are shown in Figure 3. The FTIR spectra show an infrared active Cu(I)−O vibrational band at 620 cm^{-1} for Oh. A small shift in the characteristic Cu(I)−O band from 620 to 614 cm^{-1} in the case of DHP and 610 cm^{-1} in the case of EHP was observed due to the crystallization and growth process.[15] The band at 1550 cm^{-1} is typical of a carboxylate group obtained from the corresponding acid which remains adsorbed on the surface of the metal oxide after the reaction of the precursor. These peaks are most pronounced in the case of the Cu_2O nanoparticles obtained from the basic medium, lesser for the case of neutral medium, and negligible for the acidic medium, which shows the extent of deprotonation of the carboxylate group, that is, the medium effect.

Field Emission Scanning Electron Microscopy (FESEM), Transmission Electron Microscopy (TEM), and

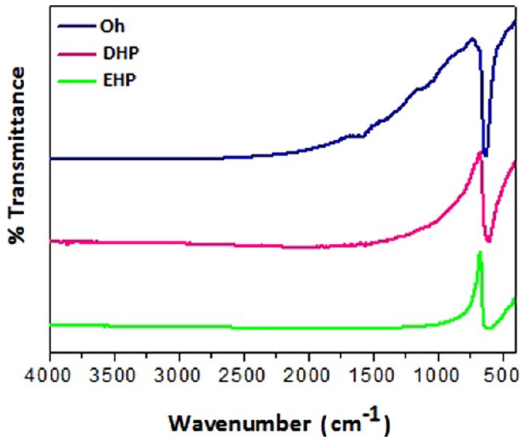

Figure 3. FTIR spectra of the three as-prepared Cu_2O morphologies.

High-Resolution (HR) TEM Analysis. The tailored morphology of the Cu_2O nanoparticles was carefully investigated under FESEM and TEM, as represented in Figures 4 and 5, respectively. Each Oh was made of triangular faces, the height of which was around 800 nm, the apex was around 300 nm in width and the base around 1 μm. Each DHP had six triangular shaped pods attached at the center, each triangle was around 2 μm in height from the center. Each pod was triangular in shape, around 500 nm in width toward the apex, and 2 μm at the base. In the case of EHP, each hexapod had a length of 20 μm, the apex was around 2 μm, and the base around 2.5 μm. The six hexapods were loosely attached at the center and a few broken pods were also observable. Eight (111) faces were exposed in the Oh structure of Cu_2O and twenty four such faces in the case of the hexapod.[31] This crystallographic orientation shows a higher catalytic activity. Hence, the higher the number of (111) faces present in the catalyst, the greater should be its activity, along with other factors evident to some extent from the nitroarene reductions carried out. It was observed that in basic NaOH medium, only the Oh structure was synthesized, whereas in acetic acid medium, the EHP structure was produced. It can be concluded that in strongly basic medium, growth of the (100) plane takes place and stops at Oh, whereas in very low basic medium, further DHP structures are formed, and with increasing acidity, the hexapod becomes elongated. However, in the presence of EG, the (100) planes do not seem

DOI: 10.1021/acsomega.6b00447
ACS Omega 2017, 2, 1968−1984

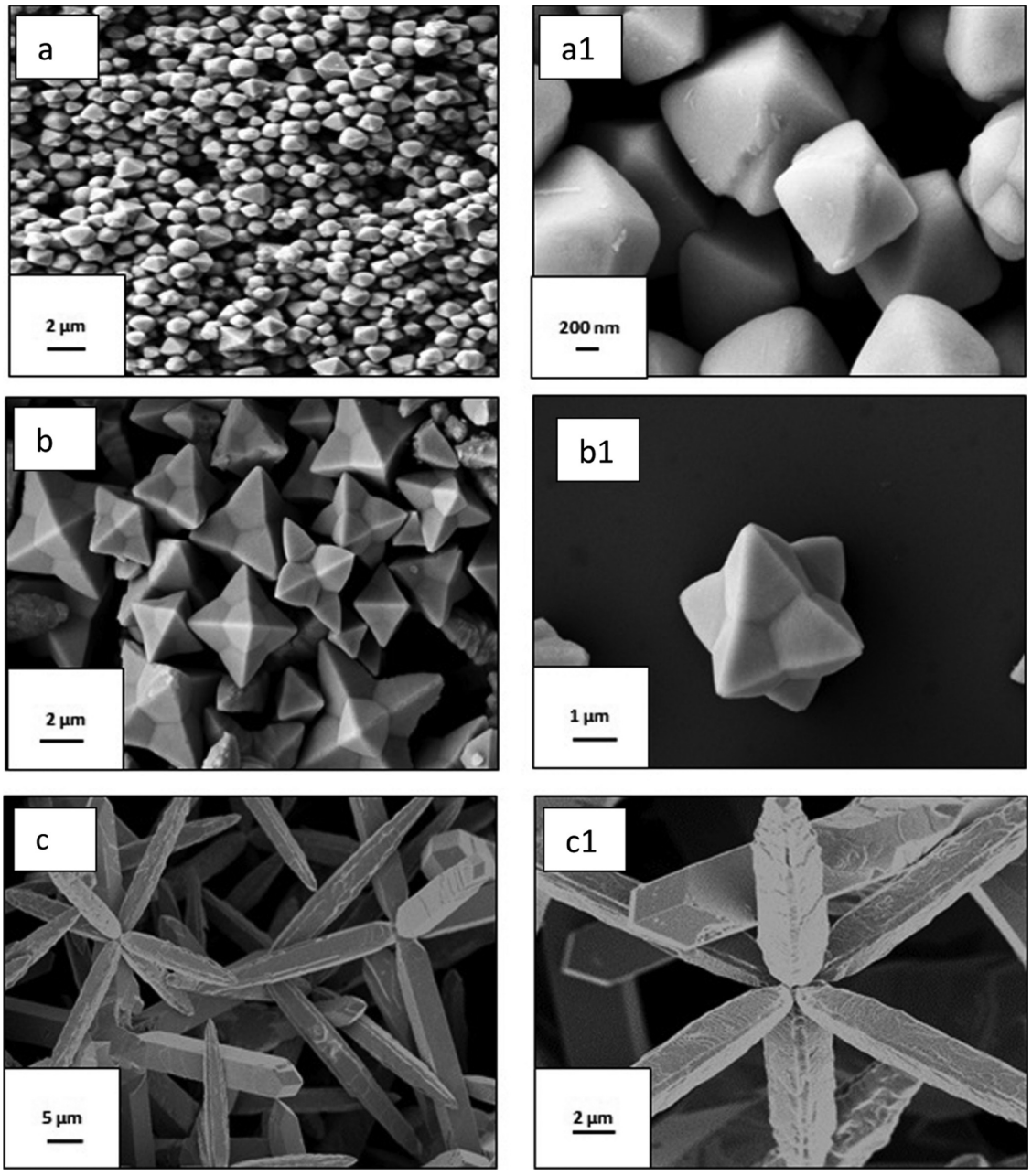

Figure 4. Low and high magnification FESEM images of Oh (a, a1), DHP (b, b1), and EHP(c, c1) morphologies of Cu_2O.

to be visible. Crystal growth is also closely related to the surface energy of the crystal face. A crystal grows rapidly in the direction perpendicular to the face that has the highest surface energy.[39] The higher growth rate of six equivalent dipolar unstable facets leads to the six branches of the extended hexapod[40] of Cu_2O when the reaction medium changes from basic to acidic. From the TEM and HRTEM images (Figure 5), the fringe was calculated with a *d*-spacing of around 2.53, 2.57, and 2.65 nm, respectively for Oh, DHP, and EHP, which can be indexed to the (111) plane, and was confirmed by SAED pattern. They also proved the presence of pure Cu_2O. FESEM images of the growth mechanism of the arrested reaction at different time intervals of all three morphologies were also studied [Figure 6a–c]. FESEM, TEM, and HRTEM analysis of the Cu_2O cube nanoparticle is also provided and clearly shows the cube morphology with fringe spacing in accordance with the Cu_2O compound [Figure S1b,c].

Energy-dispersive X-ray (EDX) Analysis. From EDX analysis, we confirmed the presence of copper and oxygen (Figure S4), the Cu peak is almost double the peak of O proving the probable composition of the nanoparticles synthesized to be Cu_2O.

Brunauer–Emmett–Teller (BET) Analysis. The FESEM and TEM images clearly display a disparity in surface area of the three different morphologies. The smaller the size of a particle, the greater the surface area. Measurements acquired from nitrogen adsorption–desorption isotherms corroborate the surface area. Figure S5a–c represents the nitrogen adsorption–desorption isotherms of the Oh, DHP, and EHP Cu_2O nanocatalysts, and the calculated BET surface areas obtained were 26.9, 11.3, and 4.3 $m^2\ g^{-1}$, respectively. The Barrett–Joyner–Halenda method was implemented for pore volume/diameter distribution, and this was found to be 0.056, 0.008, and 0.007 cc g^{-1}, with pore diameters of 14.8, 15.6, and

DOI: 10.1021/acsomega.6b00447
ACS Omega 2017, 2, 1968–1984

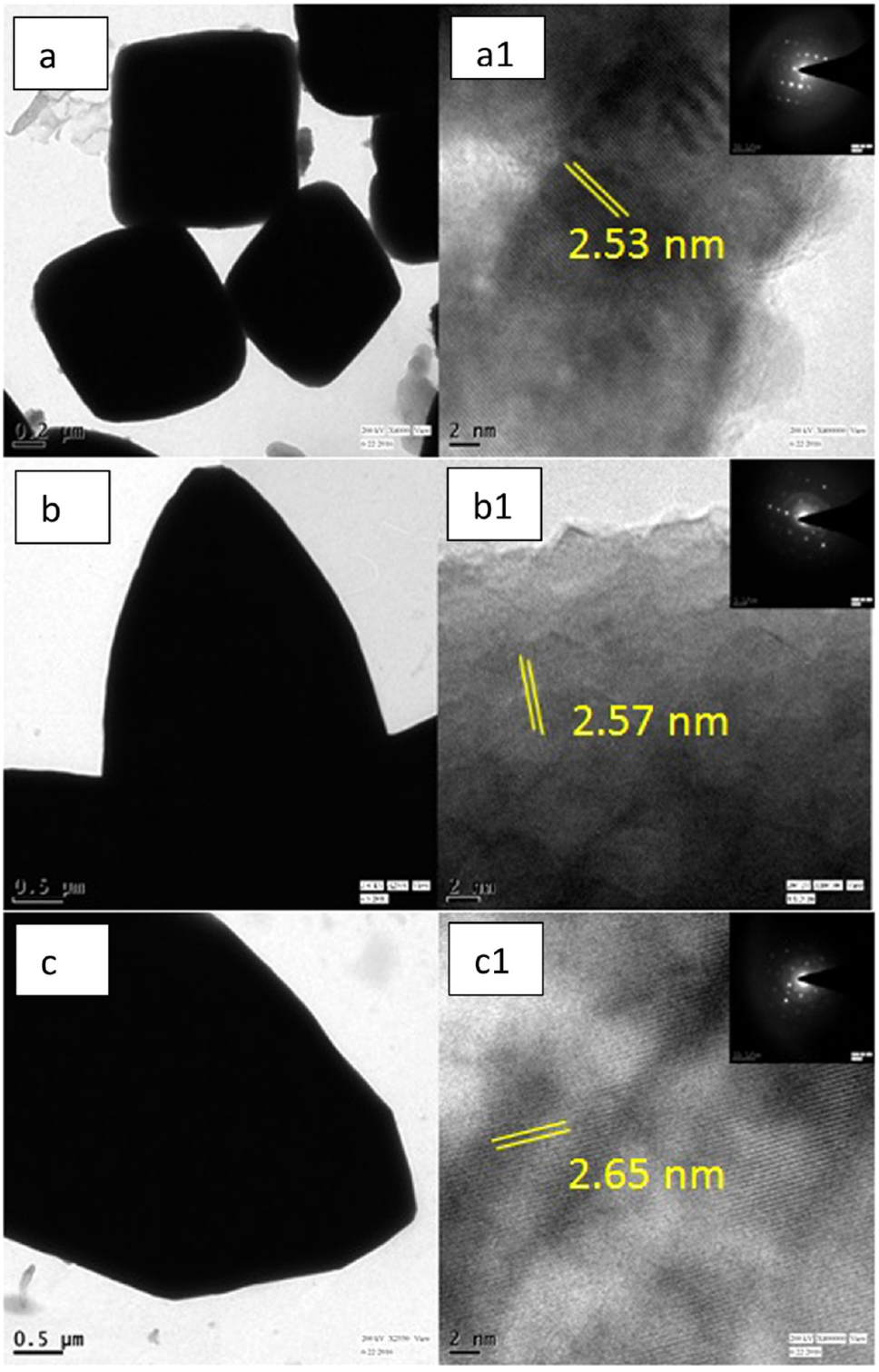

Figure 5. TEM and HRTEM images and SAED (inset) pattern, respectively, of (a, a1) Oh, (b, b1) DHP, and (c, c1) EHP morphologies of Cu_2O.

15.6 Å for Oh, DHP, and EHP, respectively. Hence, the surface area of Oh was higher than that of DHP and EHP. The order of surface area established was Oh > DHP > EHP. Again, when compared with the cube, we observed that the surface area was close to the Oh samples, 20.6 $m^2\ g^{-1}$, the pore diameter being 15.6 Å [Figure S5d].

Synthesis of Cu_2O. Our work combines the effects of EG and glucose to form hierarchical structures at variable pH due to a medium effect. On carrying out the synthesis with EG and glucose, the optimum concentration was evaluated for the Oh, DHP, and EHP structure evolution. The Cu(II) precursor salt was stirred for an hour with a stabilizer, EG, with no change in pale blue aqua complex color proving that reduction does not occur here with the free hydroxyl groups, and only the Cu(II)−EG complex is formed. We carried out the reaction in basic (pH ∼ 9.0), neutral (pH ∼ 7.0), and acidic (pH ∼ 6.0) media. No other copper salts were able to give the product in neutral and acidic media under similar conditions. The reduction

DOI: 10.1021/acsomega.6b00447
ACS Omega 2017, 2, 1968−1984

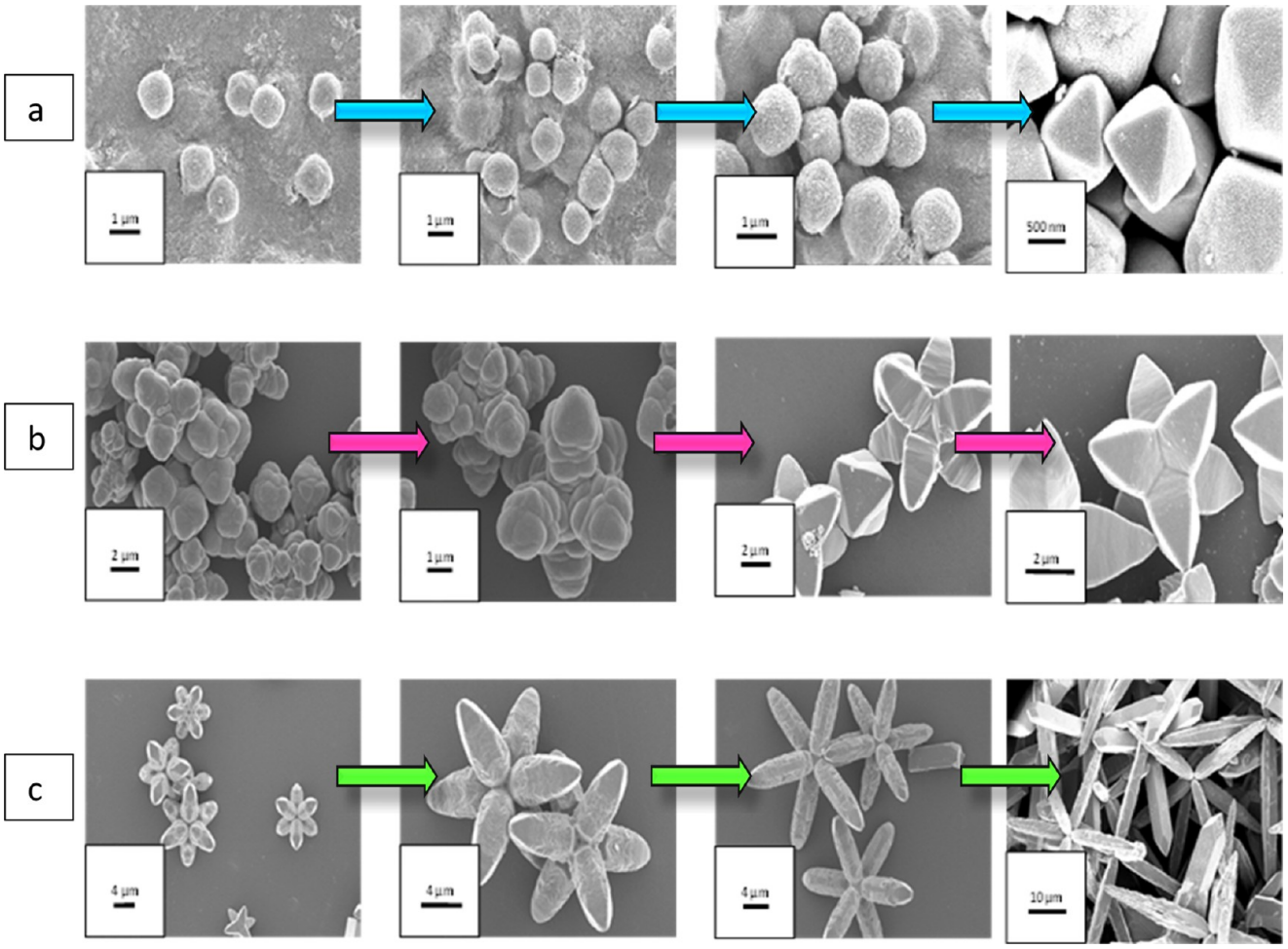

Figure 6. Growth steps taken at 3, 6, 10 h, and final product, respectively, for (a) Oh, (b) DHP, and (c) EHP morphologies of Cu_2O.

potential of the Cu^{2+}/Cu^{+} system is E_0 = 0.158 V and that of the gluconic acid/glucose system is E_0 = 0.05 V. Hence, in view of the reduction potential values, glucose is predicted to reduce the cupric state to cuprous, and in turn, glucose is oxidized to gluconic acid.[41] The probable steps of the reaction are schematically represented in Scheme 1.

Scheme 1. Schematic Representation of the Synthesis of Cu_2O from Copper Acetate Solution in the Presence of EG and Glucose under MHT Conditions

$$\text{Cu(II)–EG complex} \rightarrow \text{Cu(OH)}_2$$

$$\text{Cu(OH)}_2 + \text{glucose} \rightarrow \text{Cu}_2\text{O}\downarrow + \text{gluconic acid}$$

Temperature control and autogenic pressure are vital for the unique morphology evolution. The combination of EG, glucose, and cupric acetate facilitates the structures with exposed (111) facets such as Oh and hexapod. Also, heating the mixture with only EG yielded both CuO and Cu_2O, and with only glucose yielded Cu_2O solely, as validated by the XRD patterns (Figure S6), but all with ill-defined structures. This proves that EG helps in forming the Cu(II)–EG complex and in the absence of glucose being a weak reducing agent, it forms CuO upon dehydration of the $Cu(OH)_2$ species[42] and also reduces some Cu(II) to Cu_2O under MHT. However, in the presence of glucose, which is a stronger reducing agent, $Cu(OH)_2$ is directly reduced to Cu_2O, without any trace of CuO. In the absence of glucose, the products formed are ill-defined, whereas in the absence of EG, the structures are distorted and not fully formed at the end of the stipulated time. In the absence of the optimum amount of EG and glucose, the product is precluded from being synthesized in neutral and acidic medium. It is also pertinent to mention that when the Oh is treated with acidic pH, when the EHP is treated in a basic pH, or when the DHP is treated with the respective concentration of NaOH and acetic acid, no interchange of structures took place in any of the cases. Hence, the prerequisite for the three different morphology evolutions is their respective pH at the commencement of the reaction. After the product is formed, a change in pH does not cause an interconversion of morphology. A synergy exists between EG and glucose to bring about the reduction of Cu(II) and the specific uniform morphology of Cu_2O.

Mechanistic Insight into the Growth of the Structures. In our prescribed pH (9.0–6.0) conditions, $Cu(OAc)_2$ converts to Cu_2O via $Cu(OH)_2$ formation. Under MHT, dehydration and reduction of the $Cu(OH)_2$ species takes place and Cu_2O is obtained.[42] The evolution of $Cu(OH)_2$ nuclei is more prevalent in at higher pH. Anyway, $Cu(OH)_2$ is the initial product of the hydrolysis of $Cu(OAc)_2$ for all three cases. At higher pH, oriented attachment defines the Oh particles because of the higher number of available Cu_2O nanoparticles. The presence of Cu_2O nanoparticles at 5 and 10 h was confirmed by XRD

DOI: 10.1021/acsomega.6b00447
ACS Omega 2017, 2, 1968–1984

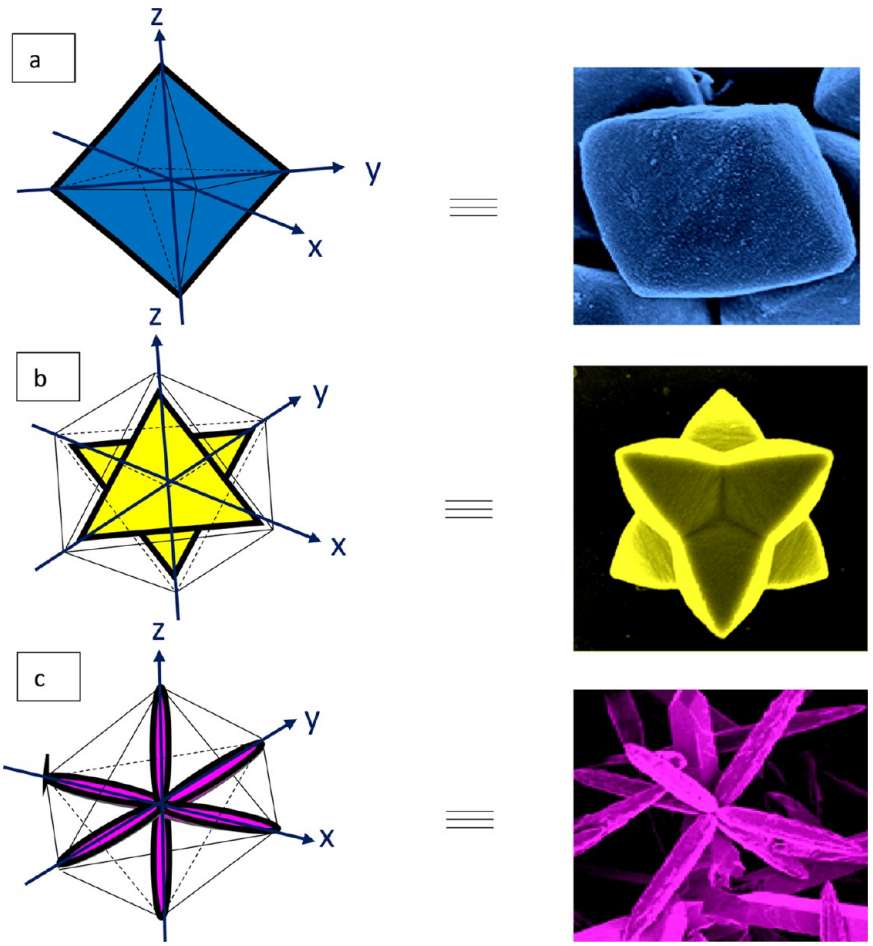

Figure 7. Schematic representation of growth along *X*, *Y*, and *Z* axes of (a) Oh, (b) DHP, and (c) EHP morphologies.

analysis, as shown in Figure S2. Hence, this authenticates our presumption that a Cu_2O nucleus is the beginning of the growth mechanism in each of the reaction mixtures and gradually evolves to different morphologies in different pH media. In the neutral to acidic conditions, fewer Cu_2O particles are generated as a result of the slow kinetics of the hydrolysis of $Cu(OAc)_2$. Thus Ostwald ripening,[43] even though already in force, and the coalescence and oriented attachment[44] mechanisms become more pronounced, and as a result of which, the DHP structure is obtained. It is worth mentioning that no other copper salts gave Cu_2O in neutral and acidic media, proving that $Cu(OAc)_2$ has an inherent tendency to ionize into $Cu(OH)_2$ species in solution, which is an intermediate in the reaction. The products obtained from MHT were all withdrawn after 18 h, however the parity in kinetics of the hydrolysis of $Cu(OAc)_2$ results in the rapid formation of fully molded Oh in basic medium within 14 h and slower rates of formation of perfectly shaped DHP and EHP at 17 and 18 h, respectively. Maintaining the reaction for longer (48 h) did not alter any of their morphologies.

The final product formation was accompanied by a number of transient steps which led gradually to the hierarchical morphology, as evident from Figure 6a–c. In the case of Oh, from 3 h under MHT, there starts a gradual evolution of Cu_2O nuclei that take up the Oh shape by Ostwald ripening from within the solution. They further modify to become spherical-shaped with emerging edges and gradually form perfect Oh structures of around 800 nm size at 14 h. There lies four apexes at the four corners of the XY plane and two other apexes at the positive and negative end of the *Z* axis that define a perfect Oh. In the case of DHP, Ostwald ripening causes small particles to evolve from the reaction mixture and the ill-defined structures of Cu_2O nuclei begin to coalesce and undergo oriented attachment, a common clue for crystal growth, at 3 h. Through constant growth and surface reconstruction, larger hexapods with smooth faces grew. Then, there occurred the simultaneous evolution of structures that vaguely form six attached Oh shapes at 6 h, which gradually extended their apexes at 10 h, and meticulously formed the symmetrical DHP structure at around 17 h. The structure's faces are a further development of the octahedral framework. Of the six hexapods, four heads lie in the *XY* plane and can be accounted back to the four apexes in the case of a pure Oh. The other two are extensions of the two apexes in the *Z* axis in the positive and negative directions. In the case of EHP, at around 3 h product formation initializes. Primarily short hexapod structures are formed by Ostwald ripening, coalescence, and oriented attachment of the pods, which is observable between 6 and 10 h. These transitory morphologies with time gradually etch, extend and mold into EHP structures at 18 h. In this case also, the six pods can be attributed to the six apexes of the Oh framework, which elongate further to give rise to the EHP. Hence, the formation of the hierarchical structures can be attributed to Ostwald ripening, coalescence, and orientated attachment, as represented in Figure S7. The orientation and growth along the axes are elucidated in the schematic representation in Figure 7a–c.

DOI: 10.1021/acsomega.6b00447
ACS Omega 2017, 2, 1968–1984

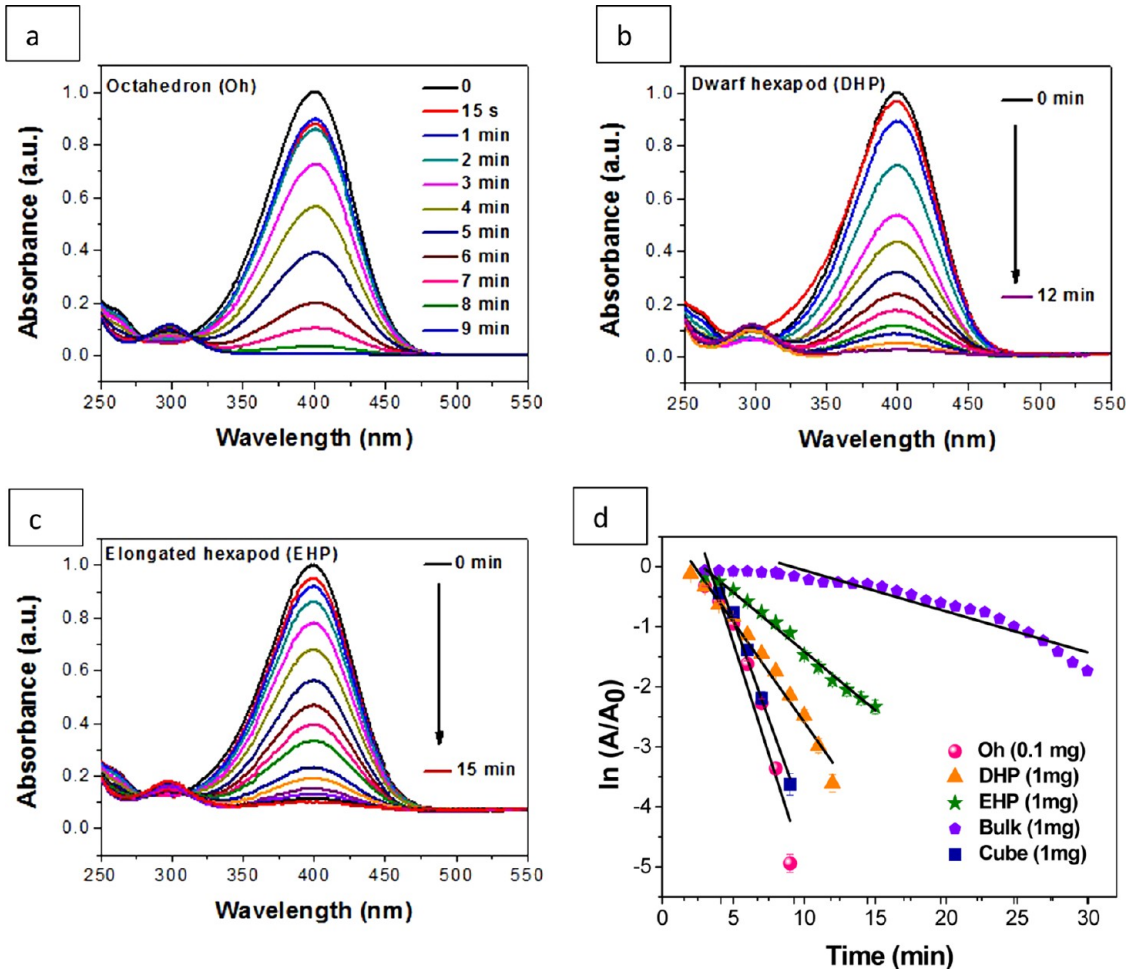

Figure 8. UV−vis absorption spectra of 4-NP reduction with (a) 0.1 mg of Oh and 1 mg of (b) DHP and (c) EHP morphologies of the as-prepared Cu_2O nanocatalysts. (d) Graph of $\ln(A/A_0)$ vs time giving the comparative rate constants of the three morphologies along with bulk Cu_2O and cube morphology with the (100) facet.

Catalytic Performance of the Cu_2O Nanostructures. A popular line of investigation of a catalyzed chemical reaction is its correlation with morphology[45−49] and facet-selection.[50−55] Bulk Cu_2O is a p-type semiconductor with a band gap value of 2.2 eV. The catalytic activity of the as-synthesized Cu_2O nanoparticles and different chemically etched products has a close relationship with the exposed particle size, surface area, crystal planes, and surface charge. To study the efficiency and ability of the as-prepared Cu_2O Oh, DHP, and EHP nanostructures, we performed hydrogenation reactions of six nitro compounds using $NaBH_4$ as the reducing agent and source of hydrogen, and the reduction of Cr(VI) to Cr(III) in the presence of FA.

Nitroarene Reduction. Nitroarenes are toxic, making it necessary to improvise methods for their transformation.[56] The reduction of nitrophenol to aminophenol has been executed directly with noble metals.[57−59] The reaction does not proceed favorably in the absence of a suitable catalyst (Figure S8). However, noble metals are not only expensive but also scarce in nature. Hence, designing alternative, low cost, abundantly available catalysts is necessary for the reaction. This has been pursued by a number of groups who have synthesized noble metal-free[60] and also metal-free catalysts.[61] Our work is the first report where morphologically variable Cu_2O using $Cu(OAc)_2$, EG, and glucose under definite pH, has been judiciously employed to reduce nitroarenes at a momentous rate. Comparative catalytic analysis of the time-dependent absorption spectra of the reduction of 4-NP to 4-aminophenol (4-AP) using $NaBH_4$ as reducing agent and adding morphologically different Cu_2O into an identical reaction medium, as the active catalyst, was performed.

First, we studied the reaction of 4-NP in solution. In an aqueous medium, a pale yellow-colored 4-NP solution shows an absorption peak at ∼317 nm (Figure S9). However, in the presence of freshly prepared $NaBH_4$, the solution becomes bright yellow and shows a strong red-shifted absorption peak at ∼400 nm due to the formation of an extended conjugation of nitrophenolate anions in alkaline medium. In the presence of catalyst as the reduction progresses, the band at 400 nm diminishes and a concomitant characteristic peak rises at ∼300 nm, which is that of colorless 4-AP. Two isosbestic points are observed at ∼311 and ∼280 nm, which confirm a clean conversion and yield of a single product.[62] To testify this, we also collected ^1H NMR data of the product obtained after the catalytic reduction of 4-NP (Figure S10). The reaction can be monitored conveniently with a UV−vis spectrophotometer. To conduct a comparative investigation of the different morphologies of Cu_2O, we separately employed the catalyst in individual identical reaction media. In each case, we obtained absorption spectra that can be further modified to obtain the

DOI: 10.1021/acsomega.6b00447
ACS Omega 2017, 2, 1968−1984

Table 1. Comparative Study of the Pseudo-First-Order Rate Constants for 4-NP Reduction with As-Prepared Cu_2O and Other Reported Nanomaterials

entry	catalyst	rate constant (k) s^{-1}	catalytic activity parameter ($k_a = k/m$) g^{-1} s^{-1}	reference
1	co-carbon composite	7.0×10^{-3}	25.9	63
2	Pd−graphene nanohybrid	2.33×10^{-3}	11.65	64
3	Cu_2O−Cu−CuO	10.4×10^{-3}	20.7	65
4	Au−Fe_3O_4	10.1×10^{-3}	11.22	66
5	Ag-nanoparticle/C	1.69×10^{-3}	1.69	67
6	Fe_3O_4−Au	1.05×10^{-2}	5.25	66
7	Pd−rGO	4.5×10^{-3}	15.0	68
8	EHP Cu_2O	3.28×10^{-3}	3.28	this work
9	DHP Cu_2O	5.59×10^{-3}	5.59	this work
10	Oh Cu_2O	1.236×10^{-2}	123.6	this work

rate constant from a $\ln(A/A_0)$ versus time graph, which demonstrates a straight line with a negative slope. We studied the time-dependent reduction kinetics by systematically preparing the reaction medium with a respective amount of catalyst (0.1 mg quantity for Oh, 1 mg quantity for DHP, EHP, bulk and cube Cu_2O), 5×10^{-5} M 4-NP, and 1.6×10^{-3} M freshly prepared $NaBH_4$ in a quartz cuvette at room temperature. The reducing agent $NaBH_4$ was added in excess (almost $\sim 10^2$ times higher in concentration than that of the substrate, 4-NP). Hence, the reaction follows pseudo-first-order reaction kinetics with a very negligible induction period. Figure 8a−c represents the UV−vis absorption spectra of the 4-NP reduction employing Oh, DHP, and EHP nanostructures, respectively. The absorption spectra of bulk Cu_2O and cubic Cu_2O nanomaterials for comparative study are given in Figure S11a,b. The plot of $\ln(A/A_0)$ versus time [Figure 8d] reveals a straight line with a negative slope, where A is the absorbance of the nitrophenolate during the progress of the reaction and A_0 is the initial absorbance of nitrophenolate before the onset of the reduction reaction. From this plot, comparative rate constants were found to be 0.742 min^{-1} ($R^2 = 0.99$) for 0.1 mg Oh catalyst, and 0.335 min^{-1} ($R^2 = 0.98$), 0.197 min^{-1} ($R^2 = 0.97$), 0.071 min^{-1} ($R^2 = 0.96$), and 0.658 min^{-1} ($R^2 = 0.97$) for 1 mg of the DHP, EHP, bulk, and previously reported cubic[15] Cu_2O catalyst, respectively. We can also define the catalytic efficiency by the catalyst activity parameter (k_a) [ratio of rate constant (k) in s^{-1} and catalyst dose (m) in g, i.e., $k_a = k/m$], which is 123.6, 5.59, 3.28, 0.81, and 10.97 g^{-1} s^{-1} for the Oh, DHP, EHP, bulk, and cubic Cu_2O catalysts. Hence, the order of efficiency is Oh > cube > DHP > EHP > bulk. From Figure 8d, the marked increase in catalytic activity is observable moving from bulk to micrometer to nanometer scale particles making the catalytic efficiency in the nanoregime more evident in comparison to that of the bulk Cu_2O. The superiority of our as-prepared (111) faceted Oh Cu_2O is evident from the comparative study of previous reports, as shown in Table 1. The activation energy for the reaction carried out with the Oh Cu_2O nanocatalyst, which catalyzes the reaction best, was as low as 22.186 kJ mol^{-1} (Figure S12) calculated from the Arrhenius equation $k = A e^{-E_a/(RT)}$, where k is the temperature-dependent rate constant, A is the pre-exponential factor, E_a is the activation energy of the reaction, R is the gas constant 8.314 J K^{-1} mol^{-1}, and T is the temperature in kelvin.

The mechanisms proposed in previous reports[18] explain that the catalysis of 4-NP occurs in two steps, first, adsorption of the substrate and second, desorption of the product, involving the catalyst. In this respect, the factors indispensable for elucidating the efficiency of a catalyst are the morphology of the nanocatalyst, active surface area for catalysis, facets involved, and the existing surface charge. Hence, a fine tuning of the morphology, facet, and increase in the surface area of a nanoparticle consequently increases the active site of the catalyst in the reaction medium, which has a direct effect on the catalytic activity. The surface area of a particle increases with its decreasing size. From the FESEM and TEM images, and BET analysis, the difference in the surface area of the nanoparticles is undisputable, and is highest for the smaller sized Oh when compared to that of DHP, which is lower, and EHP, which is least. Figure 9 establishes a linear relationship of rate constants

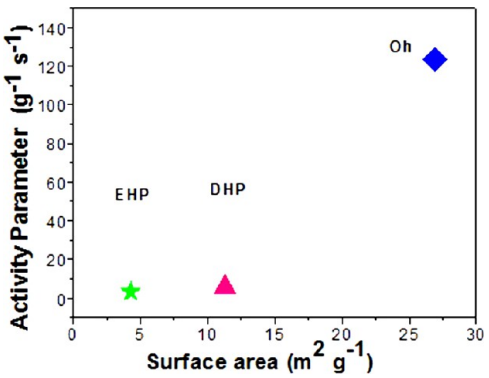

Figure 9. Linear relationship between the surface area of the as-prepared catalysts and the catalyst activity parameter.

with the surface areas of the morphologies, as obtained from BET analysis (Figure S5), proving that the greater the surface area of the catalyst, the better the efficiency, thereby validating the adeptness of the Oh Cu_2O nanocatalyst over the DHP and EHP Cu_2O nanocatalysts, all bearing the (111) facet. Because of the variance in the surface area of the three different morphologies, the same (111) faceted Oh Cu_2O nanocatalyst with 26.9 m^2 g^{-1} surface area has a higher number of catalytically active Cu(I) sites, with respect to DHP with 11.3 m^2 g^{-1} and EHP with 4.3 m^2 g^{-1} surface areas. The increased active sites increases the surface area of reaction to a great extent for the Oh, a lesser extent for the DHPm and least for the EHP morphology. Also, the higher the rate of adsorption of the substrate on the surface of the catalyst, the greater the expected rate. This was also validated by turn over frequency calculated for ~65% conversion of 5×10^{-5} M 4-NP solution using the Oh, DHP, and EHP nanocatalysts individually, the values obtained being 0.325×10^{-5}, 0.271×10^{-6}, and 0.181×10^{-6} mol g^{-1} s^{-1}, respectively. Thereafter, we observed that the surface area of cubic Cu_2O (20.6 m^2 g^{-1}), though close to that

DOI: 10.1021/acsomega.6b00447
ACS Omega 2017, 2, 1968−1984

of the Oh, still shows less efficiency. Hence, the significance of facet and surface charge is manifested in the comparison of the rate constants of Oh and cubic Cu_2O. In a typical Cu_2O body-centered cube (BCC) unit, each oxygen atom is surrounded by tetrahedron Cu atoms, whereas each Cu atom is surrounded by two oxygen atoms. On slicing the BCC unit diagonally, in the exposed (111) plane, every two Cu atoms have a dangling bond perpendicular to the plane, which leads to unsaturated Cu in the facet, which is highly active, providing a positive surface, in comparison to the (100) facet which has almost a neutral surface. The zeta potential (ζ) data of the three as-prepared morphologies, along with the cube, support the above statement and follow the order Oh (∼+30.9 mV) > DHP (∼+22.1 mV) > EHP (∼+9.53 mV) > cube (∼+2.04 mV), performed with very low (0.025 mg per 1 mL) concentration of Cu_2O in a well-dispersed ethanol medium. The positive ζ potential of the (111) facet agrees well with the crystal plane analysis, whereas a mildly positive to neutral charge is expected for the (100) facet. The surface charge of the Oh is highest, whereas that of the DHP, EHP, and cube are lower.[47] From the data, it is evident that all of the structures formed in the presence of copper acetate, EG, and glucose under MHT, but differing in active surface area and surface charge have (111) faces exposed. The exposed active Cu(I) site, surface charge, and active surface area are instrumental in bringing about the remarkable catalytic behavior of the (111) faceted Oh Cu_2O due to favorable and enhanced adsorption of nitroarene. Next, we explain explicitly how the catalytic activity of the (111) plane is greater when compared to that of the (100)[69−71] plane in specific reactions. A comparative account of the experimental results provides another vital illustration, as the (111) faceted Oh Cu_2O catalyzed the reduction with greater propensity when compared to catalysis by the (100) faceted cube [FESEM, TEM, and HRTEM images in Figure S1b,c] of similar size, that is, ∼500−800 nm. The point of zero charge (PZC) of the Oh Cu_2O nanoparticle was calculated to be at pH 10.85 [PZC graph in Figure S13], which is evidence of the positive surface charge of the nanoparticle and its high adsorbing tendency toward anionic species. The rich copper exposed (111) facet facilitates the formation of a highly active positive surface in alkaline solution,[72] as is the condition prevailing in the nitrophenol reduction reaction with $NaBH_4$. The high adsorption of the anionic deprotonated nitrophenolate on the surface of the positively charged and more accessible Cu atom of the Cu_2O nanoparticle is complimentary for the formation of the Cu−nitrophenolate active species and hence an increase in reaction rate is irrefutable in the case of the Oh morphology. The greater the positive surface charge and number of active sites of (111) facets, the more competent the catalyst is. 4-NP reduction on this selected facet has been proved unequivocally from the above discussion. Additionally, to evaluate the efficiency of the catalyst toward 4-NP reduction in the presence of other anions, we introduced Cl^-, NO_2^-, NO_3^-, CO_3^{2-}, and SO_4^{2-} (Figure 10), at 5 times lower concentration than that of 4-NP, into the reaction medium. The movement of an anion in a solution is dependent on the size of the ion and its effective charge. Hence, if the ion is small, then it will diffuse at a faster rate and adsorb on the surface of the catalyst. Again, the greater the effective charge of the ion, the higher its affinity toward the positively charged surface of the catalyst. The smaller ions, due to their size, easily move through the solution to reach the positively charged surface, thereby retarding the adsorption of nitrophenolate. However, the decrease in the rate of the

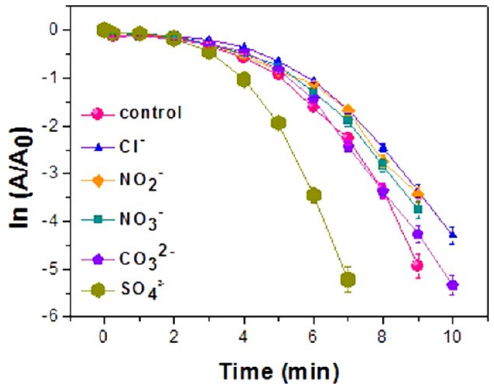

Figure 10. Effect of anions on 4-NP reduction with $NaBH_4$ in aqueous medium.

reaction was not very high due to the strong affinity of the resonance stabilized nitrophenolate on the (111) facet. The SO_4^{2-} ion is the largest among all of the other ions and hence, in spite of having a more effective charge it is incapable of diffusing to the surface of the catalyst. However, in this case, the rate is increased considerably. This is similar to the "salting out" phenomenon and the rate enhancement is observed because of the relatively stronger attachment caused by the forced confinement of the nitrophenolate ion on the surface of the catalyst due to bulky anions in the vicinity. Therefore, the observed result conveys two occurrences: (i) the diffusibility of the smaller ions causing retardation of the reaction rate due to competitive adsorption of the small anions on the positively charged surface of the nanocatalyst, and (ii) the bulky ions which diffuse at a slower rate but assist in supporting the 4-NP adsorbed on the surface of the nanocatalyst enhancing the reaction rate, in comparison to the controlled reaction.

Hereafter, we used the Oh catalyst for further studies. For an insightful investigation into the contribution of the catalyst, we varied the catalyst amount, $NaBH_4$ concentration, and 4-NP concentration, as shown in Figure S14a,a1,b,b1,c,c1. The optimized reaction conditions were determined from Figure S14d.

Hence, it is noteworthy that a low-cost catalyst with a highly active facet is most complimentary in bringing about the facile reduction of nitrophenol. To extend this explanation to the case of other nitroarenes, we selected five compounds with structurally divergent groups with substitutions at different positions in the ring, keeping all of the conditions unaltered. As the order of reactivity of the different morphologies was noted to be Oh > DHP > EHP, the rest of the reductions were performed with a minimal quantity of 0.1 mg of the nanocatalyst with the Oh structure, for feasibility of measurement, and to study in detail the effects of the catalyst on the reduction reaction. We observed that the nitroarene reduction occurred rapidly within 3−7 min keeping all other conditions unchanged, as shown in Figure 11. On comparing the compounds it was observed that 3-nitroaniline showed the maximum reactivity. As we have found previously, the reaction goes through the nitrophenolate ion, which is stabilized by resonance[21] due to the presence of an electron-withdrawing nitro group. Hence, we can assume that 4-NP is more stable with respect to 2-nitrophenol due to steric effects. A similar explanation holds well for 2-nitroaniline and 4-nitroaniline, which are both stabilized by resonance, but the former is less stable than the latter due to steric effects. However, 3-

DOI: 10.1021/acsomega.6b00447
ACS Omega 2017, 2, 1968−1984

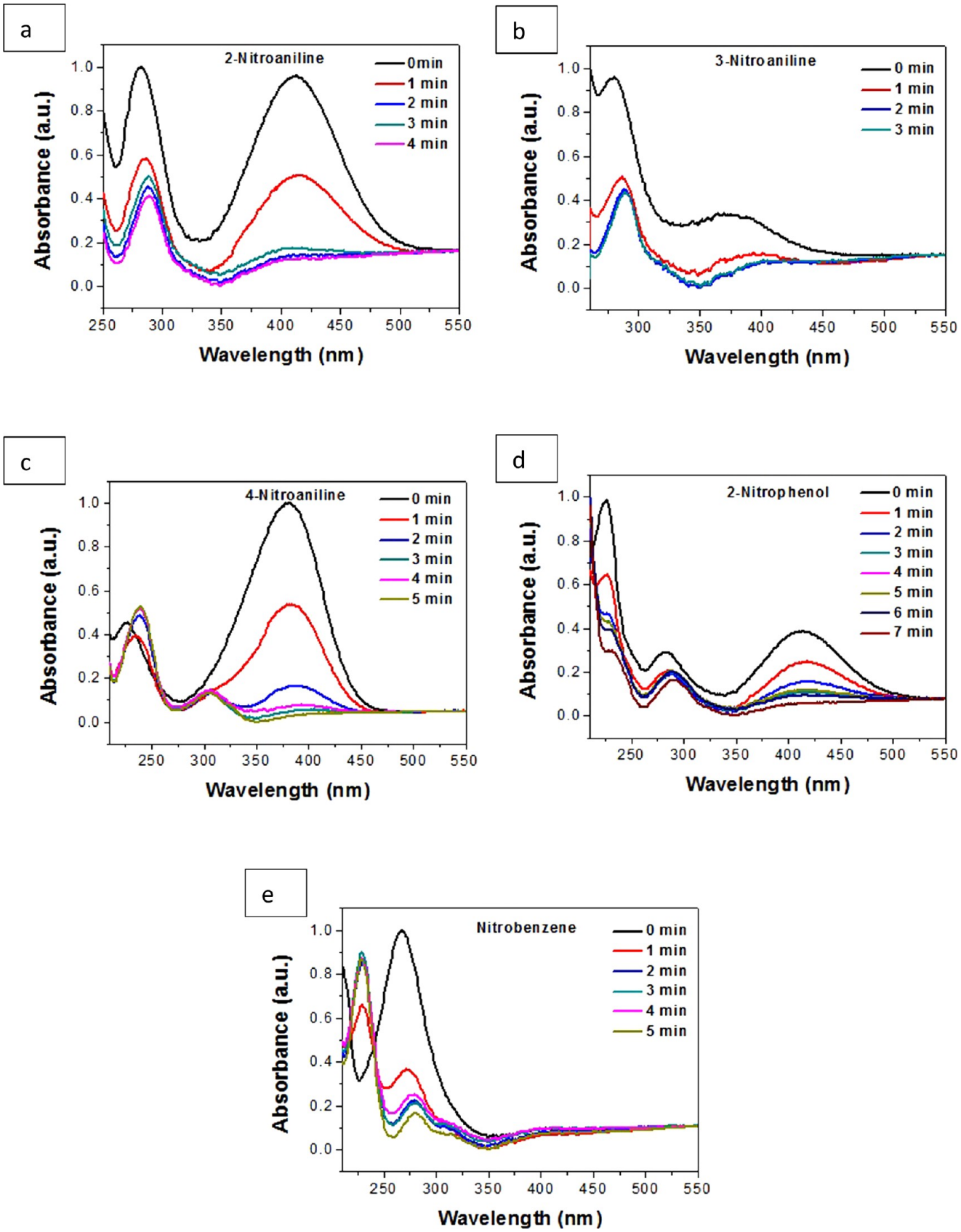

Figure 11. UV−vis absorption spectra of (a) 2-nitroaniline, (b) 3-nitroaniline, (c) 4-nitroaniline, (d) 2-nitrophenol, and (e) nitrobenzene.

nitroaniline is the least stable as there is no resonance stabilization. The nitroarene ions that have the least stability have the highest reactivity, which is evident from the very small reduction time required, as is evident from the absorption spectra. For the present study, it is important to comprehend the chemistry executed on the surface of the metal oxide

DOI: 10.1021/acsomega.6b00447
ACS Omega 2017, 2, 1968−1984

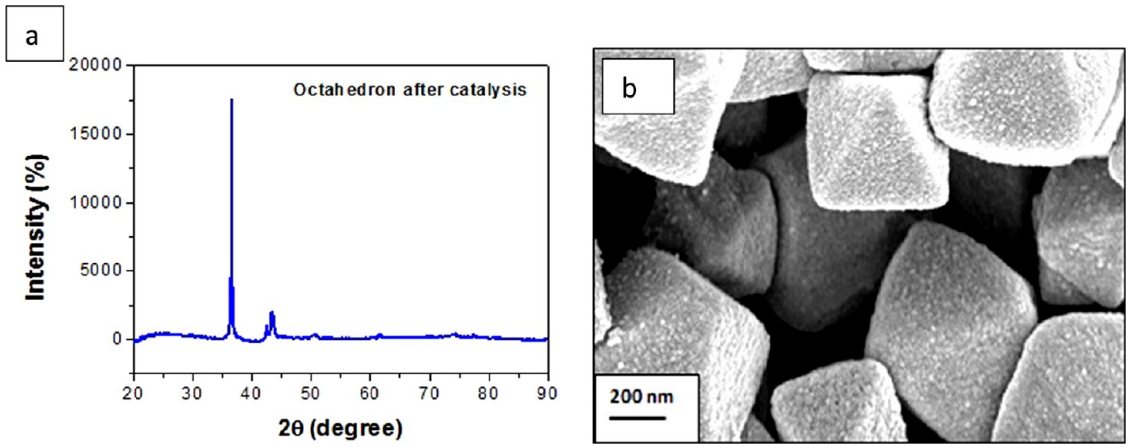

Figure 12. (a) XRD pattern and (b) FESEM images of the as-synthesized Oh Cu_2O nanocatalyst after the completion of 4-NP reduction reaction.

catalyst. It may be inferred from the observations described that not only the surface area but also the facets providing active sites for reaction and the surface charge collectively bestow upon the catalyst its efficiency. As per the crystal structure, the active surface area estimation from BET analysis, PZC, and ζ potential values, it can be assumed that the Cu atoms with dangling bonds are active toward the negatively charged molecules. From previous reports it can be presumed that the nitroarene reduction takes place on the surface of the active catalyst and the mechanism proposed is that whereby the reducing agent $NaBH_4$ and the substrate get attached on the surface of the catalyst. The Cu_2O molecules produce an in situ Cu(0) species which is highly active toward the reduction reaction.[65] The negatively charged species of borohydride and nitrophenolate adsorb on the surface of the catalyst rapidly and immediate onset of the reduction process occurs, which can be attributed to the lack of or negligible induction time, when the catalyst amount is 1 mg. However, with a decrease in the catalyst quantity to as low as 0.1 mg, a visible induction period in the absorption spectra is witnessed. The borohydride ion interacts with Cu(0) and transfers a surface hydrogen molecule, along with electrons, to it, causing the reduction of the $-NO_2$ group of nitroarene to an $-NH_2$ group. The role of the active surface area, facet, and the surface charge are pertinent for facile reactivity. The Cu_2O produces Cu(0) and presumably it is also oxidized to form CuO[73] in the alkaline medium (pH ∼ 9.84) of the reaction, which gradually causes a diminished efficiency. On adsorption of the molecules on the surface of the catalyst, the scaffold for a facile hydrogenation process is improvised and as a result of which, the nitrophenol gets reduced by the hydrogen produced in situ from borohydride in the vicinity. The catalytic performance of the as-prepared Cu_2O was investigated by repeating the same reaction under similar conditions with the preused catalyst. $NaBH_4$ is a strong reducing agent and was present in excess in the reaction medium, hence the catalytic cycle of the as-prepared catalyst is hampered after some cycles of reaction. The XRD patterns [Figure 12a] of the used catalyst show peaks of Cu_2O with the (111) peak becoming stronger and more eminent with respect to the other peaks which confirms the reduction of Cu_2O to Cu(0) metal and back to Cu_2O after catalyzing the reduction in alkaline medium. However, new peaks of Cu(0) are also evident due to a gradual reduction of Cu_2O to Cu(0) due to the usage of a strong reducing agent like $NaBH_4$. The remarkable catalysis was completed without any change in morphology of the catalyst proving its stability and robustness, as evident from Figure 12b, after 20 cycles. The catalyst retains its efficiency to a great extent, even after 20 cycles, with a weight loss of ∼45% of 1 mg catalyst taken, as evident from the $\ln(A/A_0)$ versus time graph (Figure S15).

Cr(VI) Reduction. Cr(VI) is one of those heavy metals that are a potential threat to the ecosystem, additionally being a carcinogen and mutagen too.[74,75] Disposal of highly soluble Cr(VI) ions from industrial waste, such as that from leather and dye manufacturing factories, into water directly causes a fatal scenario for terrestrial life.[76,77] However, Cr(III), being a less toxic element, can be conveniently precipitated out from solution and easily adsorbed into the soil.[78] The elimination of Cr(VI) to produce Cr(III) by adsorption or reduction[79,80] is of great importance to contemporary chemists and environmentalists. The simplistic protocol using FA is generally preferred in the presence of various metal nanocatalysts, as this technique does not produce any harmful pollutants from its byproducts.[81,82] In the absence of any catalyst, FA is unable to reduce Cr(VI) (Figure S16). The absorbance at 350 nm is the evidence of a ligand-to-metal charge transfer, which diminishes with time due to progress of the reduction reaction. The color of the solution changes from yellow to colorless at the experimental concentration range indicating the successful conversion to Cr(III)[83] with effective reduction in the presence of catalyst and reaches its completion in almost 50 min. We also calculated and compared the rate constant of the reaction with the Oh and cube Cu_2O nanocatalysts from the $\ln(A/A_0)$ versus time plot for the absorbance taken at 350 nm [Figure 13]. As the FA concentration is excessively higher (∼3600 times) than that of $K_2Cr_2O_7$, the reaction is expected to follow pseudo-first order kinetics. The successful reduction confirms the effective decomposition of FA which helps in the reduction of Cr(VI). The facet selectivity of reactions can effectively define the activity of the nanocatalyst in this case. There was an upsurge in the decrease of Cr(VI) ions in the solution for the cube rather than Oh Cu_2O nanocatalysts, the calculated activity parameters (k_a) being 4.1 g^{-1} s^{-1} (R^2 = 0.98) and 2.0 g^{-1} s^{-1} (R^2 = 0.99), respectively. We can observe a difference in the rate constants of our Oh Cu_2O nanocatalyst and cube Cu_2O, which clearly proves the facet selective reactivity. Presumably, Cr(VI) is preferentially adsorbed on the (100) facet of Cu_2O rather than the (111) facet. Hence, the (100) facet of cube, being neutral, consolidates the reduction of Cr(VI) more efficiently than does the (111) facet of the Oh. This explanation is valid as long as

DOI: 10.1021/acsomega.6b00447
ACS Omega 2017, 2, 1968−1984

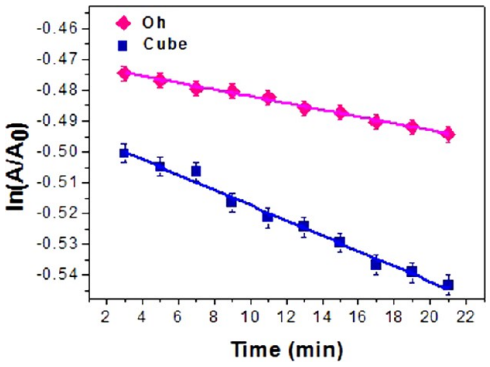

Figure 13. Comparative plot of $\ln(A/A_0)$ vs time, at 350 nm wavelength of Cr(VI) using the Oh and cube Cu_2O nanocatalysts.

undissociated dichromic acid remains present in the FA medium. So, the formic acid can reduce Cr(VI) to Cr(III) through the Cu_2O surface, which forms in situ Cu(0) and reverts back to Cu(I). However, this conversion is not as facile in acid medium as in basic medium, like that prevailing in 4-NP reaction. As a result, the catalyst gets exhausted after its use for about four cycles. The XRD pattern and FESEM images [Figure 14a,b] are provided and prove that Cu_2O is gradually reduced to Cu(0) after prolonged use of the catalyst in FA medium. Though the rate constant is low, being an inexpensive material our nanocatalyst is economically favorable when compared to costly Pd nanocatalysts.[84] Hence, the catalyst stands out as an effective robust catalyst for the reduction of toxic Cr(VI) to less toxic Cr(III) ions. The low rate constant value is indicative of the low efficiency of the (111) facet toward the removal of dichromate, thus advocating the reaction specificity of the (111) facet of Cu_2O as inferred from the investigation.

We can circumscribe the observations from both reactions to being due to a facet specific phenomenon. As the surface area of the Oh and cube Cu_2O are comparable, the rapid reactivity of the Oh catalyst can only be justified through its facet. The zeta potential values and PZC are indicative of the rapid reaction of the negatively charged molecules on the surface of the (111) plane, whereas the effect is not significant for positively charged molecules. Hence, the (111) facet is a better scaffold for nitrophenol reduction, whereas the (100) facet facilitates Cr(VI) reduction. A plausible cause for such an observation could also be the structure of the substrates. Nitrophenolate formed in basic medium, as $NaBH_4$ is in excess, is an anionic species with its electron density delocalized along the extended conjugation making the molecule more likely to be adsorbed on the positive surface of the (111) facet with respect to the neutral (100) facet. Now, in the case of Cr(VI) degradation, the medium for the reaction is acidic and hence the O^- ends of the two bound tetrahedral units of the dichromate molecule are saturated with H^+ in the vicinity. The only available Cr^{6+} in the dichromate species is therefore adsorbed on the electronegative O atoms of the exposed (100) facet. In the case of the (111) facet, the Cu atoms are exposed, hence the surface is already positive and the adsorption of a Cr(VI) center is not considerably facile. Hence, the reaction specific efficiency of the facet is well manifested in the experimental observations.

CONCLUSIONS

In a nutshell, we have synthesized three different hierarchical morphologies of Cu_2O with the (111) facet, using EG as a stabilizing agent, and glucose as a growth directing agent. However, both are instrumental, collaboratively, for reduction under different pH conditions and exert a synergy that is absolutely necessary to bring about the unique morphologies of a Cu_2O nanomaterial of different particle sizes but with the same (111) facet. The synthetic process generates the tailored growth of the Cu_2O nanoparticles systemically directing the size, morphology, and exclusively exposed facet. All of the prepared nanomaterials demonstrated excellent catalytic activity toward nitroarene reduction without any additive or promoter for the reaction. We have also illustrated that in the nanoregime, apart from the particle size, the active facet and its surface potential are contributory for the high efficiency of the catalyst. The combined effect of the size, surface area, catalytically active (111) facet, and surface charge are the key features for the simplistic reduction of nitroarenes by $NaBH_4$. The efficiency of the reduction reaction was assessed in the presence of other interfering anions that were 5 times lower in concentration than that of 4-NP. We concluded that the bulky anions promote the reaction due to their inability to diffuse toward the catalyst surface and their ability to confine the already adsorbed nitrophenolate species for facile reaction. However, the smaller ions deter it due to their high diffusibility in the solution and affinity for the positively charged (111) facet of the Oh Cu_2O. The versatility of the catalyst lies in the

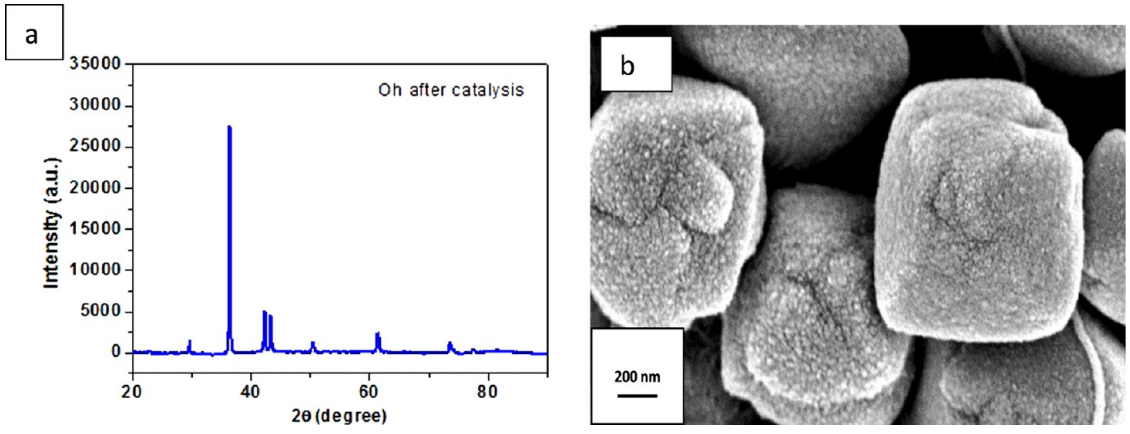

Figure 14. (a) XRD pattern and (b) FESEM images of the as-synthesized Oh Cu_2O nanocatalyst after the completion of the Cr(VI) reduction reaction.

DOI: 10.1021/acsomega.6b00447
ACS Omega 2017, 2, 1968−1984

fact that it is able to catalyze two different reactions effectively; that of 4-NP by $NaBH_4$ and Cr(VI) in the presence of FA. The manifestation of the surface charge of the nanocatalyst and their inveterate facet selectivity were established by the difference in rate constants of both reactions when compared using the dissimilar (111) and (100) faceted Cu_2O. The ease of operation of the catalyst, brief reaction period, convenient reaction conditions, and aqueous medium present the catalyst as an economical, green, and eco-friendly material for promoting a myriad of reactions. Further, a tailored facet could bestow increasing efficacy to the same nanocatalyst by many folds for predictable specific reactions. The remarkable efficiency of the as-prepared Cu_2O nanocatalyst consorted with its morphological stability makes it an ace nanocatalyst for contemporary applications in nanotechnology.

EXPERIMENTAL SECTION

Chemicals. All chemicals used were of AR grade. Details are provided in the Supporting Information.

Synthesis of Cu_2O Oh, DHP, and EHP. In a typical synthesis, 7.5 mL of 0.1 M copper (II) acetate was stirred with 2.5 mL of EG for 1 h in a magnetic stirrer at 500 rpm. From this mixture, an 8 mL aliquot was withdrawn and poured separately into a screw capped test tube. Then, 2 mL of water and 1 mL of 0.1 M glucose solution were also added to the mixture. The screw capped test tubes were sealed properly with Teflon tape after being capped. They were then kept under our laboratory designed MHT reactor under 200 W electric bulb illumination for 18 h of heating at a temperature of about 120 °C. The brown precipitate of obtained DHP was washed several times with water and then with ethyl alcohol. It was then dried and used for further characterization.

Two more sets of reactions were prepared in basic (with respect to NaOH, pH ∼ 9.0) and acidic (with respect to acetic acid, pH ∼ 5.0) media. The concentrations of all of the reagents were identical to those mentioned above, only in one of the screw capped test tubes, 0.1 M NaOH was added whereas in the other, 0.1 M acetic acid was added, to maintain the basic and acidic conditions, respectively. The screw capped test tubes were then wrapped properly with Teflon tape. They were then kept in the MHT reactor under 200 W electric bulb illumination for 18 h at a temperature of about 120 °C. The former yielded the dark brown Oh and the latter yielded dark brown EHP Cu_2O nanomaterial. All of these brown precipitates were also washed with water and ethanol, and dried for further characterization.

Catalytic Reduction of 4-NP. In a typical reaction, 1.5 mL of 10^{-4} M aqueous solution of nitroarene and 500 μL of freshly prepared 10^{-2} M $NaBH_4$, which resulted in concentrations of 5×10^{-5} and 1.6×10^{-3} M, respectively, in the solution, were mixed in a quartz cuvette under ambient conditions. Then, a respective amount of as-prepared Cu_2O nanomaterial (0.1 mg quantity for Oh, 1 mg quantity for DHP, EHP, bulk, and cube Cu_2O) was introduced individually in the reaction medium and the disappearance of the yellow color of the solution was monitored using a UV−vis spectrophotometer. This experiment was individually conducted with each of the three catalysts, namely, Oh, DHP, EHP synthesized by our novel strategy, cubic Cu_2O from the literature,[15] and bulk Cu_2O for comparative study of the 4-NP reduction. To study the effect of other common anions, we added 1.0×10^{-5} M NaCl, $NaNO_2$, $NaNO_3$, Na_2CO_3, and Na_2SO_4 solutions. We carried out the rest of the detailed study on the reduction reaction parameters and other nitroarene reductions with a minimal amount of 0.1 mg of as-obtained Oh Cu_2O nanocatalyst for an insightful investigation in five sets of reactions. The recyclability test was performed with 1 mg of Oh Cu_2O nanocatalyst for 20 cycles. All of the kinetic tests were performed and the results were provided without the influence of diffusion.

Catalytic Reduction of Cr(VI). The catalytic proficiency of the (111) faceted Cu_2O was also studied toward the reduction of hexavalent chromium, Cr(VI), using FA at room temperature. In a typical procedure, 10 mL of reaction mixture was prepared with potassium dichromate ($K_2Cr_2O_7$, 5×10^{-4} M), 1.8 M FA and 0.01 mL of Cu_2O catalyst (1 mg per 1 mL of Oh and cube Cu_2O nanocatalyst) dispersed in water and stirred magnetically at 500 rpm at room temperature. Then, a 2 mL aliquot was put in a quartz cuvette after centrifuging and separating out the present catalyst. The absorbance at 350 nm was monitored at definite time intervals to study the progress of the reaction for five sets.

ASSOCIATED CONTENT

Supporting Information

The Supporting Information is available free of charge on the ACS Publications website at DOI: 10.1021/acsomega.6b00447.

Analytical instruments, chemicals used, XRD analysis, FESEM, TEM, and HRTEM images, Auger spectra, XPS spectra, EDX analysis, N_2-adsorption−desorption plot (with pore size diameter), absorption spectra, ^{1}H NMR data, linear calibration plots, PZC plot (PDF)

AUTHOR INFORMATION

Corresponding Author

*E-mail: tpal@chem.iitkgp.ernet.in.

ORCID

Tarasankar Pal: 0000-0001-8708-2050

Notes

The authors declare no competing financial interest.

ACKNOWLEDGMENTS

The authors are thankful for financial support from the DST, UGC, and CSIR New Delhi, India, MHRD and IIT Kharagpur for financial support and research facilities, and we are also thankful to Prof. G. M. Rao (IISc Bangalore, India) for their support in XPS characterization and Prof. D. Dhara (Dept. of Chemistry, IIT Kharagpur, India) for the zeta potential measurements of the nanomaterials. The authors are also thankful to Dr. Vinod C Prabhakaran (Catalysis Division and Center of Excellence on Surface Science, CSIR-National Chemical Laboratory, Pune, India) for helpful discussions on Auger Spectroscopy.

REFERENCES

(1) Astruc, D. Transition-Metal Nanoparticles in Catalysis: From Historical Background to the State-of-the Art. In *Nanoparticles and Catalysis*; Wiley-VCH: New York, 2008.

(2) Kazes, M.; Lewis, D. Y.; Banin, U. Method for Preparation of Semiconductor Quantum-Rod Lasers in a Cylindrical Microcavity. *Adv. Funct. Mater.* **2004**, *14*, 957−962.

(3) Xu, C.; Xie, J.; Ho, D.; Wang, C.; Kohler, N.; Walsh, E. G.; Morgan, J. R.; Chin, Y. E.; Sun, S. Au-Fe_3O_4 Dumbbell Nanoparticles as Dual-Functional Probes. *Angew. Chem., Int. Ed.* **2008**, *47*, 173−176.

DOI: 10.1021/acsomega.6b00447
ACS Omega 2017, 2, 1968−1984

(4) Choi, J.-S.; Jun, Y.-W.; Yeon, S.-I.; Kim, H. C.; Shin, J.-S.; Cheon, J. Biocompatible Heterostructured Nanoparticles for Multimodal Biological Detection. *J. Am. Chem. Soc.* **2006**, *128*, 15982−15983.
(5) Feng, L.; Zhang, C.; Gao, G.; Cui, D. Facile Synthesis of Hollow Cu_2O Octahedral and Spherical Nanocrystals and Their Morphology-Dependent Photocatalytic Properties. *Nanoscale Res. Lett.* **2012**, *7*, No. 276.
(6) Sui, Y.; Fu, W.; Yang, H.; Zeng, Y.; Zhang, Y.; Zhao, Q.; Li, Y.; Zhou, X.; Leng, Y.; Li, M.; Zou, G. Low Temperature Synthesis of Cu_2O Crystals: Shape Evolution and Growth Mechanism. *Cryst. Growth Des.* **2010**, *10*, 99−108.
(7) Kuo, C. H.; Huang, M. H. Morphologically controlled synthesis of Cu_2O nanocrystals and their properties. *Nano Today* **2010**, *5*, 106−116.
(8) Ahmed, A.; Gajbhiye, N. S. Room temperature ferromagnetism in Mn, Ni and Co ions doped Cu_2O nanorods. *J. Solid State Chem.* **2010**, *183*, 3100−3104.
(9) Zhang, D.-F.; Zhang, H.; Guo, L.; Zheng, K.; Han, X.-D.; Zhang, Z. Delicate Control of Crystallographic Facet-Oriented Cu_2O Nanocrystals and the Correlated Adsorption Ability. *J. Mater. Chem.* **2009**, *19*, 5220−5225.
(10) Sui, Y. M.; Fu, W. Y.; Zeng, Y.; Yang, H. B.; Zhang, Y. Y.; Chen, H.; Li, Y. X.; Li, M. H.; Zou, G. T. Synthesis of Cu_2O Nanoframes and Nanocages by Selective Oxidative Etching at Room Temperature. *Angew. Chem., Int. Ed.* **2010**, *49*, 4282−4285.
(11) Panigrahi, S.; Kundu, S.; Ghosh, S. K.; Nath, S.; Praharaj, S.; Basu, S.; Pal, T. Selective one-pot synthesis of copper nanorods under surfactantless condition. *Polyhedron* **2006**, *25*, 1263−1269.
(12) Veeramania, V.; Sivakumara, M.; Chen, S.-M.; Madhu, R.; Daia, Z.-C.; Miyamotob, N. A facile electrochemical synthesis strategy for Cu_2O (cubes, sheets and flowers) microstructured materials for sensitive detection of 4-Nitrophenol. *Anal. Methods* **2016**, *8*, 5906−5910.
(13) Li, S.-K.; Guo, X.; Wang, Y.; Huang, F.-Z.; Shen, Y.-H.; Wang, X.-M.; Xie, A.-J. Rapid Synthesis of Flower-Like Cu_2O Architectures in Ionic Liquids by the Assistance of Microwave Irradiation with High Photochemical Activity. *Dalton Trans.* **2011**, *40*, 6745−6750.
(14) Kuo, C.-H.; Huang, M. H. Fabrication of Truncated Rhombic Dodecahedral Cu_2O Nanocages and Nanoframes by Particle. *J. Am. Chem. Soc.* **2008**, *130*, 12815−12820.
(15) Pal, J.; Ganguly, M.; Mondal, C.; Roy, A.; Negishi, Y.; Pal, T. Crystal-Plane-Dependent Etching of Cuprous Oxide Nanoparticles of Varied Shapes and Their Application in Visible Light Photocatalysis. *J. Phys. Chem. C* **2013**, *117*, 24640−24653.
(16) Tafesh, A. M.; Weiguny, J. A Review of the Selective Catalytic Reduction of Aromatic Nitro Compounds into Aromatic Amines, Isocyanates, Carbamates, and Ureas Using CO. *Chem. Rev.* **1996**, *96*, 2035−2052.
(17) Shi, Q.; Lu, R.; Lu, L.; Fu, X.; Zhao, D. Efficient Reduction of Nitroarenes over Nickel-Iron Mixed Oxide Catalyst Prepared from a Nickel-Iron Hydrotalcite Precursor. *Adv. Synth. Catal.* **2007**, *349*, 1877−1881.
(18) Aditya, T.; Pal, A.; Pal, T. Nitroarene reduction: a trusted model reaction to test nanoparticle catalysts. *Chem. Commun.* **2015**, *51*, 9410−9431.
(19) Pradhan, N.; Pal, A.; Pal, T. Catalytic Reduction of Aromatic Nitro Compounds by Coinage Metal Nanoparticles. *Langmuir* **2001**, *17*, 1800−1802.
(20) Sarkar, S.; Sinha, A. K.; Pradhan, M.; Basu, M.; Negishi, Y.; Pal, T. Redox Transmetalation of Prickly Nickel Nanowires for Morphology Controlled Hierarchical Synthesis of Nickel/Gold Nanostructures for Enhanced Catalytic Activity and SERS Responsive Functional Material. *J. Phys. Chem. C* **2011**, *115*, 1659−1673.
(21) Wunder, S.; Polzer, F.; Lu, Y.; Mei, Y.; Ballauff, M. Kinetic Analysis of Catalytic Reduction of 4-Nitrophenol by Metallic Nanoparticles Immobilized in Spherical Polyelectrolyte Brushes. *J. Phys. Chem. C* **2010**, *114*, 8814−8820.
(22) Layek, K.; Kantam, M. L.; Shirai, M.; Nishio-Hamane, D.; Sasakid, T.; Maheswarana, H. Gold Nanoparticles Stabilized on Nanocrystalline Magnesium Oxide as an Active Catalyst for Reduction of Nitroarenes in Aqueous Medium at Room Temperature. *Green Chem.* **2012**, *14*, 3164−3174.
(23) Khalavka, Y.; Becker, J.; Sönnichsen, C. Synthesis of Rod-Shaped Gold Nanorattles with Improved Plasmon Sensitivity and Catalytic Activity. *J. Am. Chem. Soc.* **2009**, *131*, 1871−1875.
(24) Johnson, J. A.; Makis, J. J.; Marvin, K. A.; Rodenbusch, S. E.; Stevenson, K. J. Size-Dependent Hydrogenation of p-Nitrophenol with Pd Nanoparticles Synthesized with Poly(amido)amine Dendrimer Templates. *J. Phys. Chem. C* **2013**, *117*, 22644−22651.
(25) Kalekar, A. M.; Sharma, K. K. K.; Lehoux, A.; Audonnet, F.; Remita, H.; Saha, A.; Sharma, G. K. Investigation into the Catalytic Activity of Porous Platinum Nanostructures. *Langmuir* **2013**, *29*, 11431−11439.
(26) Antonels, N. C.; Meijboom, R. Preparation of Well-Defined Dendrimer Encapsulated Ruthenium Nanoparticles and Their Evaluation in the Reduction of 4-Nitrophenol According to the Langmuir−Hinshelwood Approach. *Langmuir* **2013**, *29*, 13433−13442.
(27) Mondal, C.; Sasmal, A. K.; Yusuf, S. M.; Mukadam, M. D.; Pal, J.; Ganguly, M.; Pal, T. Modified hydrothermal reaction (MHT) forCoV2O6$4H2O nanowire formation and the transformation to CoV2O6$2H2O single-crystals for antiferromagnetic ordering and spin-flop†our lab paper. *RSC Adv.* **2014**, *4*, 56977−56983.
(28) Sahoo, R.; Roy, A.; Dutta, S.; Ray, C.; Aditya, T.; Pal, A.; Pal, T. Liquor ammonia mediated V(V) insertion in thin Co3O4 sheets for improved pseudocapacitors with high energy density and high specific capacitance value. *Chem. Commun.* **2015**, *51*, 15986−15989.
(29) Liu, G.; Jimmy, C. Y.; Lu, G. Q. M.; Cheng, H.-M. Crystal facet engineering of semiconductor photocatalysts: motivations, advances and unique properties. *Chem. Commun.* **2011**, *47*, 6763−6783.
(30) Xiong, Y.; Xia, Y. Shape-Controlled Synthesis of Metal Nanostructures: The Case of Palladium. *Adv. Mater.* **2007**, *19*, 3385−3391.
(31) Shang, Y.; Guo, L. Facet-Controlled Synthetic Strategy of Cu_2O-Based Crystals for Catalysis and Sensing. *Adv. Sci.* **2015**, *2*, No. 1500140.
(32) Ho, J.-Y.; Huang, M. H. Synthesis of Submicrometer-Sized Cu_2O Crystals with Morphological Evolution from Cubic to Hexapod Structures and Their Comparative Photocatalytic Activity. *J. Phys. Chem. C* **2009**, *113*, 14159−14164.
(33) Liu, X.-W.; Wang, F.-Y.; Zhen, F.; Huang, J.-R. In Situ Growth of Au Nanoparticles on the Surfaces of Cu_2O Nanocubes for Chemical Sensors with Enhanced Performance. *RSC Adv.* **2012**, *2*, 7647−7651.
(34) Zheng, Z.; Huang, B.; Wang, Z.; Guo, M.; Qin, X.; Zhang, X.; Wang, P.; Dai, Y. Crystal Faces of Cu_2O and Their Stabilities in Photocatalytic Reactions. *J. Phys. Chem. C* **2009**, *113*, 14448−14453.
(35) Yin, M.; Wu, C. K.; Lou, Y.; Burda, C.; Koberstein, J. T.; Zhu, Y.; O'Brien, S. Copper Oxide Nanocrystals. *J. Am. Chem. Soc.* **2005**, *127*, 9506−9511.
(36) Wang, W.; Wang, G.; Wang, X.; Zhan, Y.; Liu, Y.; Zheng, C. Synthesis and Characterization of Cu_2O Nanowires by a Novel Reduction Route. *Adv. Mater.* **2002**, *1*, 67−69.
(37) Sohn, Y.; Pradhan, D.; Zhao, L.; Leung, K. T. Anomalous Oxidation Resistance of "Core-Only" Copper Nanoparticles Electrochemically Grown on Gold Nanoislands Prefunctionalized by 1,4-phenylene Diisocyanide. *Electrochem. Solid-State Lett.* **2012**, *15*, K35−K39.
(38) Sung, M. M.; Sung, K.; Kim, C. G.; Lee, S. S.; Kim, Y. Self-Assembled Monolayers of Alkanethiols on Oxidized Copper Surfaces. *J. Phys. Chem. B* **2000**, *104*, 2273−2277.
(39) Gasparotto, A.; Barreca, D.; Maccato, C.; Tondello, E. Manufacturing of inorganic nanomaterials: concepts and perspectives. *Nanoscale* **2012**, *4*, 2813−2825.
(40) Xu, H.; Wang, W.; Zhu, W. Shape Evolution and Size-Controllable Synthesis of Cu_2O Octahedra and Their Morphology-Dependent Photocatalytic Properties. *J. Phys. Chem. B* **2006**, *110*, 13829−13834.

DOI: 10.1021/acsomega.6b00447
ACS Omega 2017, 2, 1968−1984

(41) Muralikrishna, S.; Sureshkumar, K.; Yan, Z.; Fernandez, T.; et al. Non-Enzymatic Amperometric Determination of Glucose by CuO Nanobelt Graphene Composite Modified Glassy Carbon Electrode. *J. Braz. Chem. Soc.* **2015**, *26*, 1632−1641.
(42) Basu, M.; Sinha, A. K.; Pradhan, M.; Sarkar, S.; Pal, A.; Mondal, C.; Pal, T. Methylene Blue−Cu_2O Reaction Made Easy in Acidic Medium. *J. Phys. Chem. C* **2012**, *116*, 25741−25747.
(43) Ostwald, W. Über die vermeintliche Isomerie des roten und gelben Quecksilberoxyds und die Oberflächenspannung fester Körper. *Z. Phys. Chem.* **1900**, *34*, 495−503.
(44) Thanh, N. T. K.; Maclean, N.; Mahiddine, S. Mechanisms of Nucleation and Growth of Nanoparticles in Solution. *Chem. Rev.* **2014**, *114*, 7610−7630.
(45) Zhang, Y.; Deng, B.; Zhang, T.; Gao, D.; Xu, A.-W. Shape Effects of Cu_2O Polyhedral Microcrystals on Photocatalytic Activity. *J. Phys. Chem. C* **2010**, *114*, 5073−5079.
(46) Hua, Q.; Cao, T.; Bao, H.; Jiang, Z.; Huang, W. Crystal-Plane-Controlled Surface Chemistry and Catalytic Performance of Surfactant-Free Cu_2O Nanocrystals. *ChemSusChem* **2013**, *6*, 1966−1972.
(47) Aditya, T.; Jana, J.; Sahoo, R.; Roy, A.; Pal, A.; Pal, T. Silver Molybdates with Intriguing Morphology and as a Peroxidase Mimic with High Sulfide Sensing Capacity. *Cryst. Growth Des.* **2017**, *17*, 295−307.
(48) Huang, W. Oxide Nanocrystal Model Catalysts. *Acc. Chem. Res.* **2016**, *49*, 520−527.
(49) Li, L.; Nan, C.; Peng, Q.; Li, Y. Selective Synthesis of Cu_2O Nanocrystals as Shape-Dependent Catalysts for Oxidative Arylation of Phenylacetylene. *Chem. Eur. J.* **2012**, *18*, 10491−10496.
(50) Chanda, K.; Rej, S.; Huang, M. H. Facet-Dependent Catalytic Activity of Cu_2O Nanocrystals in the One-Pot Synthesis of 1,2,3-Triazoles by Multicomponent Click Reactions. *Chem. Eur. J.* **2013**, *19*, 16036−16043.
(51) Bao, H.; Zhang, W.; Shang, D.; Hua, Q.; Ma, Y.; Jiang, Z.; Yang, J.; Huang, W. Shape-Dependent Reducibility of Cuprous Oxide Nanocrystals. *J. Phys. Chem. C* **2010**, *114*, 6676−6680.
(52) Hua, Q.; Shang, D.; Zhang, W.; Chen, K.; Chang, S.; Ma, Y.; Jiang, Z.; Yang, J.; Huang, W. Morphological Evolution of Cu_2O Nanocrystals in an Acid Solution: Stability of Different Crystal Planes. *Langmuir* **2011**, *27*, 665−671.
(53) Hua, Q.; Chen, K.; Chang, S.; Ma, Y.; Huang, W. Crystal Plane-Dependent Compositional and Structural Evolution of Uniform Cu_2O Nanocrystals in Aqueous Ammonia Solutions. *J. Phys. Chem. C* **2011**, *115*, 20618−20627.
(54) Huang, W.-C.; Lyu, L.-M.; Yang, Y.-C.; Huang, M. H. Synthesis of Cu_2O Nanocrystals from Cubic to Rhombic Dodecahedral Structures and Their Comparative Photocatalytic Activity. *J. Am. Chem. Soc.* **2012**, *134*, 1261−1267.
(55) Bao, H.; Zhang, W.; Hua, Q.; Jiang, Z.; Yang, J.; Huang, W. Crystal-Plane-Controlled Surface Restructuring and Catalytic Performance of Oxide Nanocrystals. *Angew. Chem., Int. Ed.* **2011**, *50*, 12294−12298.
(56) Vaidya, M. J.; Kulkarni, S. M.; Chaudhari, R. V. Synthesis of p-Aminophenol by Catalytic Hydrogenation of p-Nitrophenol. *Org. Process Res. Dev.* **2003**, *7*, 202−208.
(57) Hervés, P.; Pérez-Lorenzo, M.; Liz-Marzán, L. M.; Dzubiella, J.; Lu, Y.; Ballauff, M. Catalysis by Metallic Nanoparticles in Aqueous Solution: Model Reactions. *Chem. Soc. Rev.* **2012**, *41*, 5577−5587.
(58) Pozun, Z. D.; Rodenbusch, S. E.; Keller, E.; Tran, K.; Tang, W.; Stevenson, K. J.; Henkelman, G. A Systematic Investigation of p-Nitrophenol Reduction by Bimetallic Dendrimer Encapsulated Nanoparticles. *J. Phys. Chem. C* **2013**, *117*, 7598−7604.
(59) Hayakawa, K.; Yoshimura, T.; Esumi, K. Preparation of Gold-Dendrimer Nanocomposites by Laser Irradiation and Their Catalytic Reduction of 4-Nitrophenol. *Langmuir* **2003**, *19*, 5517−5521.
(60) Su, Y.; Lang, J.; Li, L.; Guan, K.; Du, C.; Peng, L.; Han, D.; Wang, X. Unexpected Catalytic Performance in Silent Tantalum Oxide through Nitridation and Defect Chemistry. *J. Am. Chem. Soc.* **2013**, *135*, 11433−11436.
(61) Kong, X. K.; Sun, Z. Y.; Chen, M.; Chen, Q. W.; et al. Metal-Free Catalytic Reduction of 4-Nitrophenol to 4-Aminophenol by N-Doped Graphene. *Energy Environ. Sci.* **2013**, *6*, 3260−3266.
(62) Sarkar, S.; Sinha, A. K.; Pradhan, M.; Basu, M.; Negishi, Y.; Pal, T. Redox Transmetalation of Prickly Nickel Nanowires for Morphology Controlled Hierarchical Synthesis of Nickel/Gold Nanostructures for Enhanced Catalytic Activity and SERS Responsive. Functional Material. *J. Phys. Chem. C* **2011**, *115*, 1659−1673.
(63) Hasan, Z.; Cho, D.-W.; Chon, C.-M.; Yoon, K.; Song, H. Reduction of *p*-nitrophenol by magnetic Co-carbon composites derived from metal organic frameworks. *Chem. Eng. J.* **2016**, *298*, 183−190.
(64) Wang, Z.; Xu, C.; Gao, G.; Li, X. Facile synthesis of well-dispersed Pd−graphene nanohybrids and their catalytic properties in 4-Nitrophenol reduction. *RSC Adv.* **2014**, *4*, 13644−13651.
(65) Sasmal, A. K.; Dutta, S.; Pal, T. A ternary Cu_2O−Cu−CuO nanocomposite: a catalyst with intriguing activity. *Dalton Trans.* **2016**, *45*, 3139−3150.
(66) Lin, F.-H.; Doong, R.-a. Bifunctional Au−Fe3O4 Heterostructures for magnetically recyclable catalysis of nitrophenol reduction. *J. Phys. Chem. C* **2011**, *115*, 6591−6598.
(67) Tang, S.; Vongehr, S.; Meng, X. Carbon Spheres with Controllable Silver Nanoparticle Doping. *J. Phys. Chem. C* **2010**, *114*, 977−982.
(68) Bramhaiah, K.; John, N. S. Hybrid films of reduced graphene oxide with noble metal nanoparticles generated at a liquid/liquid interface for applications in catalysis. *RSC Adv.* **2013**, *3*, 7765−7773.
(69) Xu, H.; Wang, W.; Zhu, W. Shape Evolution and Size-Controllable Synthesis of Cu_2O Octahedra and Their Morphology-Dependent Photocatalytic Properties. *J. Phys. Chem. B* **2006**, *110*, 13829−13834.
(70) Xu, Y.; Wang, H.; Yu, Y.; Tian, L.; Zhao, W.; Zhang, B. Cu_2O Nanocrystals: Surfactant-Free Room-Temperature Morphology-Modulated Synthesis and Shape-Dependent Heterogeneous Organic Catalytic Activities. *J. Phys. Chem. C* **2011**, *115*, 15288−15296.
(71) Leng, M.; Liu, M.; Zhang, Y.; Wang, Z.; Yu, C.; Yang, X.; Zhang, Z.; Wang, C. Polyhedral 50-Facet Cu_2O Microcrystals Partially Enclosed by {311} High-Index Planes: Synthesis and Enhanced Catalytic CO Oxidation Activity. *J. Am. Chem. Soc.* **2010**, *132*, 17084−17087.
(72) Liu, X.; Sui, Y.; Yang, X.; Lina Jiang, L.; Wang, F.; Wei, Y.; Bo Zou, B. A feasible approach to synthesize Cu_2O microcrystals and their enhanced non-enzymatic sensor performance. *RSC Adv.* **2015**, *5*, 59099−59105.
(73) Pal, J.; Mondal, C.; Sasmal, A. K.; Ganguly, M.; Negishi, Y.; Pal, T. Account of Nitroarene Reduction with Size- and Facet-Controlled CuO−MnO2 Nanocomposites Reduction of p-nitrophenol by magnetic Co-carbon composites derived from metal organic frameworks. *ACS Appl. Mater. Interfaces* **2014**, *6*, 9173−9184.
(74) Wise, S. S.; Shaffiey, F.; LaCerte, C.; Goertz, J.; Caroline, E. C.; Dunn, J. L.; Gulland, F. M. D.; Aboueissa, A.-M.; Zheng, T.; Wise, J. P., Sr. Particulate and soluble hexavalent chromium are cytotoxic and genotoxic to Steller sea lion lung cells. *Aquat. Toxicol.* **2009**, *91*, 329−335.
(75) Stearns, D. M.; Kennedy, L. J.; Courtney, K. D.; Giangrande, L. P. H.; Phieffer, S.; Wetterhahn, K. E. Reduction of Chromium(VI) by Ascorbate Leads to Chromium-DNA Binding and DNA Strand Breaks in Vitro. *Biochemistry* **1995**, *34*, 910−919.
(76) Prabhakaran, K.; Vijayaraghavan, K.; Balasubramanian, R. Removal of Cr(VI) Ions by Spent Tea and Coffee Dusts: Reduction to Cr(III) and Biosorption. *Ind. Eng. Chem. Res.* **2009**, *48*, 2113−2117.
(77) Mondal, C.; Ganguly, M.; Pal, J.; Roy, A.; Jana, J.; Pal, T. Morphology Controlled Synthesis of SnS_2 Nanomaterial for Promoting Photocatalytic Reduction of Aqueous Cr(VI) under Visible Light. *Langmuir* **2014**, *30*, 4157−4164.
(78) Djouider, F. Radiolytic formation of non-toxic Cr(III) from toxic Cr(VI) in formate containing aqueous solutions: A system for water treatment. *J. Hazard. Mater.* **2012**, *223−224*, 104−109.

DOI: 10.1021/acsomega.6b00447
ACS Omega 2017, 2, 1968−1984

(79) Sarkar, S.; Dutta, S.; Bairi, P.; Pal, T. Redox-Responsive Copper(I) Metallogel: A Metal−Organic Hybrid Sorbent for Reductive Removal of Chromium(VI) from Aqueous Solution. *Langmuir* **2014**, *30*, 7833−7841.
(80) Bhaumik, M.; Maity, A.; Srinivasu, V. V.; Onyango, M. S. Enhanced removal of Cr(VI) from aqueous solution using polypyrrole/Fe_3O_4 magnetic nanocomposite. *J. Hazard. Mater.* **2011**, *190*, 381−390.
(81) Gong, K.; Wang, W.; Yan, J.; Han, Z. Highly reduced molybdophosphate as a noble-metal-free catalyst for the reduction of chromium using formic acid as a reducing agent. *J. Mater. Chem. A* **2015**, *3*, 6019−6027.
(82) Zhang, R.; Liu, H.; Wang, B.; Ling, L. Insights into the Preference of CO_2 Formation from HCOOH Decomposition on Pd Surface: A Theoretical Study. *J. Phys. Chem. C* **2012**, *116*, 22266−22280.
(83) Huang, Y.; Ma, H.; Wang, S.; Shen, M.; Guo, R.; Cao, X.; Zhu, M.; Shi, X. Efficient Catalytic Reduction of Hexavalent Chromium Using Palladium Nanoparticle-Immobilized Electrospun Polymer Nanofibers. *ACS Appl. Mater. Interfaces* **2012**, *4*, 3054−3061.
(84) Celebi, M.; Yurderi, M.; Bulut, A.; Kaya, M.; Zahmakiran, M. Palladium nanoparticles supported on amine-functionalized SiO_2 for the catalytic hexavalent chromium reduction. *Appl. Catal., B* **2016**, *180*, 53−64.

DOI: 10.1021/acsomega.6b00447
ACS Omega 2017, 2, 1968−1984